Geoscience Frontiers 14 (2023) 101650

Contents lists available at ScienceDirect

Geoscience Frontiers

journal homepage: www.elsevier.com/locate/gsf

Research Paper

Empirical assessment of the role of the Sun in climate change using balanced multi-proxy solar records

Nicola Scafetta

Department of Earth Sciences, Environment and Georesources, University of Naples Federico II, Complesso Universitario di Monte S. Angelo, via Cinthia, 21, Naples 80126, Italy

ARTICLE INFO

Article history:
Received 6 March 2023
Revised 5 June 2023
Accepted 8 June 2023
Available online 14 June 2023
Handling Editor: R.D. Nance

Keywords:
Solar activity changes
Solar variability climatic impact
Global climate change and modeling
Equilibrium climate sensitivity

ABSTRACT

The role of the Sun in climate change is hotly debated. Some studies suggest its impact is significant, while others suggest it is minimal. The Intergovernmental Panel on Climate Change (IPCC) supports the latter view and suggests that nearly 100% of the observed surface warming from 1850–1900 to 2020 is due to anthropogenic emissions. However, the IPCC's conclusions are based solely on computer simulations made with global climate models (GCMs) forced with a total solar irradiance (TSI) record showing a low multi-decadal and secular variability. The same models also assume that the Sun affects the climate system only through radiative forcing – such as TSI – even though the climate could also be affected by other solar processes. In this paper I propose three "balanced" multi-proxy models of total solar activity (TSA) that consider all main solar proxies proposed in scientific literature. Their optimal signature on global and sea surface temperature records is assessed together with those produced by the anthropogenic and volcanic radiative forcing functions adopted by the CMIP6 GCMs. This is done by using a basic energy balance model calibrated with a differential multi-linear regression methodology, which allows the climate system to respond to the solar input differently than to radiative forcings alone, and to evaluate the climate's characteristic time-response as well. The proposed methodology reproduces the results of the CMIP6 GCMs when their original forcing functions are applied under similar physical conditions, indicating that, in such a scenario, the likely range of the equilibrium climate sensitivity (ECS) could be 1.4 °C to 2.8 °C, with a mean of 2.1 °C (using the HadCRUT5 temperature record), which is compatible with the low-ECS CMIP6 GCM group. However, if the proposed solar records are used as TSA proxies and the climatic sensitivity to them is allowed to differ from the climatic sensitivity to radiative forcings, a much greater solar impact on climate change is found, along with a significantly reduced radiative effect. In this case, the ECS is found to be 0.9–1.8 °C, with a mean of around 1.3 °C. Lower ECS ranges (up to 20%) are found using HadSST4, HadCRUT4, and HadSST3. The result also suggests that at least about 80% of the solar influence on the climate may not be induced by TSI forcing alone, but rather by other Sun-climate processes (e.g., by a solar magnetic modulation of cosmic ray and other particle fluxes, and/or others), which must be thoroughly investigated and physically understood before trustworthy GCMs can be created. This result explains why empirical studies often found that the solar contribution to climate changes throughout the Holocene has been significant, whereas GCM-based studies, which only adopt radiative forcings, suggest that the Sun plays a relatively modest role.

1. Introduction

The Sun's contribution to climate change is a hotly debated and controversial topic: empirical studies usually claim that it has a significant impact, while others, usually based on global climate model (GCM) simulations, claim that it has a modest effect. In this work I address this critical issue and propose a solution. The conundrum appears to stem from two sorts of uncertainties: (i) the historical solar activity multidecadal and secular variations are not precisely known; and (ii) the Sun likely influences the Earth's climate through a variety of physical mechanisms that are not fully understood yet and, therefore, are missing in the available

Abbreviations: GCM, Global Climate Model; ECS, Equilibrium Climate Sensitivity; TCR, Transient Climate Response; TSA, Total Solar Activity; TSI, Total Solar Irradiance.

E-mail address: nicola.scafetta@unina.it

https://doi.org/10.1016/j.gsf.2023.101650

GCMs. This introduction outlines the most important open issues and uncertainties on this topic.

Total solar irradiance (TSI) can only be measured using satellites, and the available TSI records began in 1978 (Willson and Mordvinov, 2003; Dewitte et al., 2004; Fröhlich, 2009; de Wit et al., 2017). As a result, in earlier times, TSI proxy models have been developed using information that could be associated with variations in solar activity such as sunspot number records, faculae indices, cosmogenic ^{14}C and ^{10}Be records, solar cycle lengths, etc. However, the proposed TSI proxy models differ greatly from one another (Hoyt and Schatten, 1993; Lean et al., 1995; Wang et al., 2005; Krivova et al., 2007, 2010; Shapiro et al., 2011; Coddington et al., 2016; Egorova et al., 2018; Wu et al., 2018; Scafetta et al., 2019; Penza et al., 2022). The main reason is that the brightness evolution of the so-called "quiet" regions of the Sun is still poorly understood. Moreover, it has also been rather challenging to calibrate and validate solar proxy models against the +40 years of TSI satellite measurements.

TSI satellite radiometers normally work for a decade or a little more, their accuracy varies significantly, and readings from different radiometers require statistical cross-calibrations before they can be integrated into a suitable long composite. So far, the TSI satellite composites continue to be contentious.

There is a major TSI-composite controversy that has not been solved yet, which has also shaped the discussion regarding the role of the Sun in climate change. Two different science teams, the Active Cavity Radiometer Irradiance Monitor (ACRIM) and the Physikalisch-Meteorologisches Observatorium Davos (PMOD), came to divergent results concerning the TSI multidecadal trend throughout the solar cycles 21–23 (roughly from 1980 to 2000). The PMOD-recommended TSI satellite composite shows a slight TSI decrease (Fröhlich and Lean, 1998; Fröhlich, 2009), while the ACRIM one shows an increase (Willson, 1997; Willson and Mordvinov, 2003): see Fig. 1. Also the so-called instrument-based "Community-Consensus TSI Composite" shows a moderate TSI increase from 1980 to 2000, followed by a slight TSI decrease (de Wit et al., 2017).

The main reason for this uncertainty is that the ACRIM-2 experiment was delayed due to the 1986 Space Shuttle Challenger incident, which prevented the new data from overlapping with the ACRIM-1 measurements. Only less precise TSI records from two alternative experiments (Nimbus/ERB and ERBS/ERBE) – which were designed for Earth Radiation Budget (ERB) investigations rather than for high precision TSI monitoring like the ACRIM ones that employed electrically self-calibrating cavity sensors – could bridge the so-called "ACRIM-gap" from 1989.5 to 1991.75, and cross-calibrate the ACRIM-1 and ACRIM-2 TSI records. The problem was that during the ACRIM-gap, the Nimbus/ERB record trended upward while the ERBS/ERBE data moderately trended downward (Scafetta and Willson, 2014).

The ACRIM science teams reasoned from an experimental standpoint and suggested that the trend shown by the Nimbus/ERB data had to be considered the most likely accurate one because NIMBUS7/ERB results were expected to be more precise than ERBS/ERBE (e.g., the instrument was measuring much more frequently) and the ACRIM-gap occurred during the peak of solar cycle 22. On the contrary, the ERBS/ERBE radiometer was expected to degrade during this solar cycle maximum because of its first exposure to high UV radiations, whereas Nimbus/ERB was launched in 1978 and its first UV exposure happened during the maximum of solar cycle 21. As a result, during the maximum of cycle 22, the Nimbus/ERB radiometer was expected to be more stable (Willson, 1997; Willson and Mordvinov, 2003).

The PMOD team, on the other hand, argued primarily from a modeling standpoint, and claimed that the upward trend indicated by the Nimbus/ERB record during the ACRIM-gap was fictitious because it appeared to diverge from the prediction of some TSI proxy models based on sunspot and faculae indices. The latter, however, only represent the so-called "active" solar regions (see the detailed discussion in Scafetta et al., 2019). On specific occasions (e.g., on September 29, 1989), radiometer "glitches" were also hypothesized to explain the observed divergences of the data from the adopted TSI proxy models. In general, the Nimbus/ERB TSI record was claimed to be affected by spurious trends and jumps that required a number of ad-hoc adjustments (Fröhlich and Lean, 1998; Fröhlich, 2009).

Consequently, ACRIM cross-calibrated ACRIM-1 and ACRIM-2 using the actual Nimbus/ERB TSI satellite published data, while PMOD did it by using a Nimbus7/ERB record that was significantly modified to replicate the slightly negative trends of the ERBS/ERBE TSI record and of some TSI proxy models. PMOD also applied calibration models built to rectify the considerable degradation of the PMO6V radiometer (on VIRGO) to the HF radiometer (on Nimbus7/ERB), assuming that the two instruments performed similarly.

However, using hypothetical methods to alter experimental results under the guise of adjusting them is always questionable. For example, the hypothesized instrumental "glitches" were investigated and dismissed by the original Nimbus/ERB experimental team because they were found physically incompatible with the experimental equipment. Douglas Hoyt, the principal investigator for the Nimbus7/ERB TSI satellite experiment, remarked: "The calibrations before and after the September shutdown gave no indication of any change in the sensitivity of the radiometer. . .. . . Fröhlich's PMOD TSI composite is not consistent with the internal data or physics of the Nimbus7 cavity radiometer" (supplementary of Scafetta and Willson, 2009). See also the independent review by Zacharias (2014).

The IPCC acknowledged the ACRIM-PMOD disagreement in its 2007 and 2013 publications (Solomon et al., 2007; Stocker et al., 2014). The most recent AR6 report (Masson-Delmotte et al., 2021), however, omitted to mention it, which could give the erroneous impression that the PMOD's adjustments of the experimental TSI data had been validated. In fact, Scafetta and Willson (2014) and Scafetta et al. (2019) presented several pieces of evidence that corroborated the ACRIM TSI composite and, more specifically, the rising trend of the Nimbus/ERB TSI record during the ACRIM-gap, such as: (i) from 1989 to 1992 the strength of the solar magnetic field continuously increased; (ii) on September 29, 1989, when the HF instrument was switched off, no "glitch" in the Nimbus7/ERB record could be identified by direct comparison with the ERBS/ERBE TSI record; (iii) the 1974–2009 TSI reconstruction by Ball et al. (2012) showed a TSI increase during the ACRIM-gap that is better correlated with the ACRIM TSI satellite composite than with the downward trend of the PMOD one; (iv) the TSI proxy models used to support the PMOD multidecadal decreasing trend (Krivova et al., 2010; Coddington et al., 2016) were found incompatible with the ACRIM-1 and ACRIM-2 TSI satellite data from 1985 to 2000, which are considered to be highly accurate.

The debate over the multidecadal trend in the TSI satellite composite has influenced both the TSI and solar spectral irradiance (SSI) proxy model reconstructions. In general, the ACRIM TSI composite implies a greater multidecadal TSI variability in contrast to the low one suggested by the PMOD TSI composite. Thus, TSI proxy models with drastically different multidecadal and secular variability have been published (Hoyt and Schatten, 1993; Lean et al., 1995; Wang et al., 2005; Shapiro et al., 2011; Vieira et al., 2011; Coddington et al., 2016; Egorova et al., 2018; Wu et al., 2018; Penza et al., 2022). They estimate that from the Maunder minimum (1645–1715) to the present, TSI might have increased from 0.75 W/m^2 to 6.3 W/m^2 (Yeo et al., 2020). This large uncer-

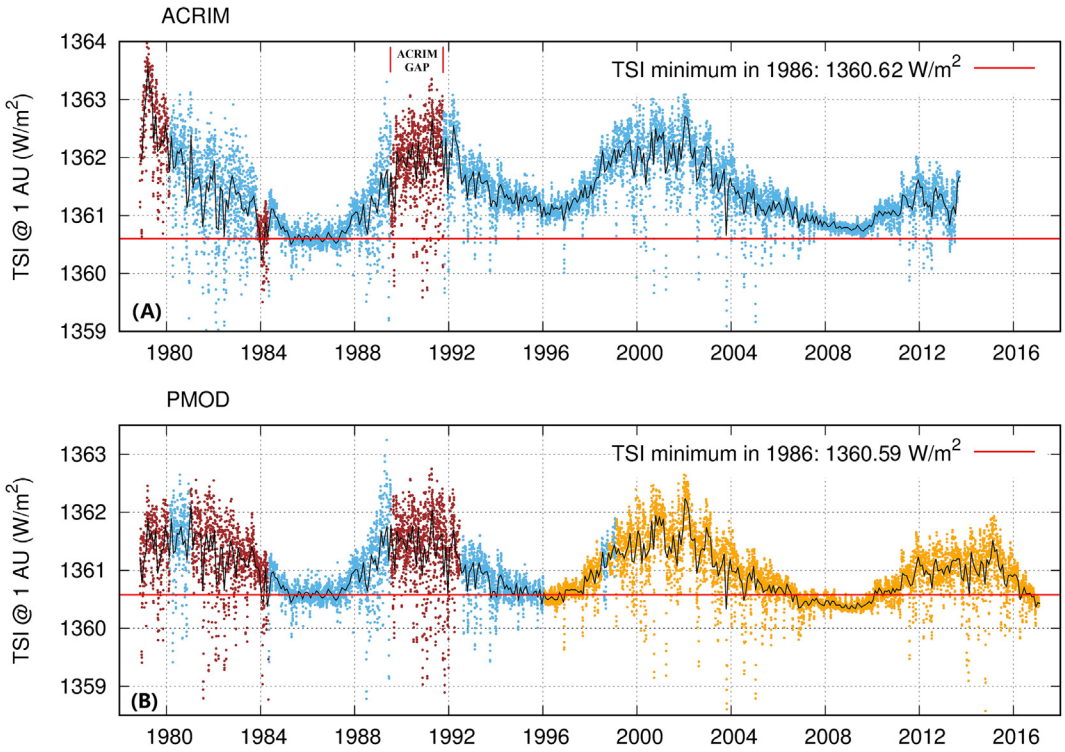

Fig. 1. (A) ACRIM TSI composite (after Scafetta and Willson, 2014). (B) PMOD TSI composite (v. 42.65.1702) (after Fröhlich, 2012). Both data sets are calibrated on the total irradiance monitor/solar radiation and climate experiment (TIM/SORCE) scale. Data from Nimbus7/Earth radiation budget (ERB; brown), ACRIM-1, ACRIM-2 and ACRIM-3 (cyan), and VIRGO (orange). (For interpretation of the references to colour in this figure legend, the reader is referred to the web version of this article.)

tainty clearly undermines any attempt to assess the Sun's role in climate change during the last centuries using GCMs whose outputs only depends on radiative-based forcings.

Some of these TSI proxy models, such as SATIRE (Krivova et al., 2007, 2010; Wu et al., 2018) and NRLTSI2 (Coddington et al., 2016)), exhibit a very modest TSI multidecadal and secular variability, and were validated against the PMOD TSI satellite composite. However, the latter was partially created by using an early version of the NRLTSI2 model (Fröhlich and Lean, 1998). Thus, the found agreement is not significant. The ACRIM TSI composite contradicts the 1980–2000 downward trend of these models. In particular, Scafetta and Willson (2014, 2019) and Scafetta et al. (2019) demonstrated that SATIRE and NRLTSI2 disagree with the TSI satellite records even when the measurements are not in dispute, as throughout the periods covered by ACRIM-1 and ACRIM-2 from 1985 to 2000. Also de Wit et al. (2017) found considerable differences between these TSI proxy models (in particular with SATIRE) and their proposed Community-Consensus TSI satellite composites. Indeed, it was discovered that if SATIRE and NRLTSI2 were empirically adjusted to optimally agree with the actual TSI satellite data during the uncontroversial periods outside the ACRIM-gap, the adjusted TSI models would fit the ACRIM rising trend from 1980 to 2000 (Scafetta and Willson, 2014; Scafetta et al., 2019).

NRLTSI2 also appears nonphysical because this TSI proxy record was created only using sunspot blocking and faculae emission indices, while the luminosity of the so-called "quiet" solar areas was supposed to be constant (Coddington et al., 2016). As a result, the modest TSI multidecadal and secular variation of NRLTSI2 might be the product of the physical assumptions of the model itself.

Other science teams used alternative solar modeling methodologies to recreate the network solar luminosity output from the allegedly "quiet" solar areas, and they concluded that solar activity could be characterized by a large multidecadal and secular variability. Hoyt and Schatten (1993), for example, developed a complex TSI proxy model based on several solar indices, which is discussed briefly in Appendix A (Supplementary Data Text). This TSI proxy model accounted for approximately 71% of the decadal variance of the Northern Hemisphere temperature anomalies from 1700 to 1992. Shapiro et al. (2011) and Egorova et al. (2018) also used a multi-proxy approach and assumed that the quiet-Sun brightness varies in time proportionally to the secular (22-year averaged) variation of the solar modulation potential. A considerable TSI variability appears to be also supported by certain astrophysical evidence. For example, Judge et al. (2020) examined a sample of 72 Sun-like stars and set a limit on the solar forcing of Earth's atmosphere equal to 4.5 W/m^2 since 1750.

Yeo et al. (2020) estimated that the dimmest state of the Sun might be 2.0 ± 0.7 W/m^2 below the 2019 level, which is more than 1 W/m^2 lower than what NRLTSI2 and SATIRE show during the Maunder minimum (1645–1715) relative to present solar cycle minima. However, such an estimate was obtained using modeling and data from modern-day solar images, which may underestimate the true dimmest level of solar luminosity because, in recent decades, solar activity appears to be oscillating around a grand solar millennium maximum (Scafetta, 2012a; Scafetta and Bianchini, 2022). Yeo et al. (2020) was also questioned by Schmutz (2021), who observed that a too low TSI secular variability could not explain the strong correlation discovered between solar and climatic records over the last centuries. According to his calculations, the found empirical correlation could require a TSI variation since the Maunder solar minimum of the order of 10 W/m^2.

Penza et al. (2022) recently proposed an alternative TSI proxy model covering the last five centuries. It also exhibits an important

secular variability, with a TSI increase from the Maunder minimum to the present equal to about 2.5 W/m^2, which is 1.5–2.0 W/m^2 more than the TSI increase shown by NRLTSI2 and SATIRE during the same period.

Despite the above considerations, NRLTSI2 and SATIRE were used by Matthes et al. (2017) to create the TSI forcing function that was adopted by the GCMs of the sixth Coupled Model Intercomparison Project Phases (CMIP6) of the World Climate Research Programme. Thus, only low-variability TSI records were used to assess the relative anthropogenic versus natural (solar and volcanic) contributions to climate change from 1850 to 2014 (Eyring et al., 2016; Masson-Delmotte et al., 2021). Moreover, the GCMs also assumed that the Sun could only affect the Earth's climate through changes in its luminosity. As a result, by using the estimated historical forcings, the CMIP6 GCMs concluded that the Sun would have made a negligible contribution to the observed global warming between 1850 and 2014.

The IPCC (Masson-Delmotte et al., 2021, AR6 page 957) ignored the high secular-variability TSI proxy reconstructions on the grounds that they rest "on assumptions about long-term changes in the quiet Sun for which there is no observed evidence". However, such an argument is questionable because there is no experimental evidence for either supporting or rejecting the secular high-variability TSI proxy reconstructions since the TSI satellite observations began in 1978 and, as discussed above, there is even disagreement over their composites.

For example, Lockwood and Ball (2020) concluded that solar activity varies little, but they did so by analyzing the TSI records since 1995 and by hypothesizing that a grand solar maximum occurred in 1985, as implied by the PMOD TSI composite. However, according to the ACRIM TSI composite, a grand solar maximum might have occurred during solar cycle 23, which began in August 1996 and ended in December 2008. Also Scafetta (2012a) suggested that a solar grand maximum might have occurred around 2000 using a solar modeling based on tidal forcing from planetary harmonics. If so, during solar cycle 23, the derivative of the multidecadal modulation of solar activity could have been at its minimum, and, therefore, the TSI trending from 1995 to 2020 could underestimate the range of the likely TSI multidecadal variations.

As further discussed below, understanding how much TSI changes at the multidecadal and secular scales may not be sufficient for climate change research. Correctly reconstructing the actual patterns of the TSI time-evolution is also essential for properly correlating specific solar activity changes to observed climate-change patterns, which could be otherwise mistaken as only a product of the chaotic internal variability of the climate system. In fact, the proposed TSI proxy models show comparable but not identical multi-decadal patterns. As a result, certain TSI proxy models appear to be better correlated with the global surface temperature records than others.

Another source of considerable uncertainty is that solar activity does not appear to influence the Earth's temperature by radiative changes alone. This is a crucial physical feature of the Sun-climate relationship that must be considered. Indeed, a vast number of paleoclimatic evidences suggests that it is the Sun's magnetic field that mostly regulates the Earth's climate (Easterbrook, 2019).

For example, cosmic rays are one example of a corpuscular forcing modulated by solar magnetic activity that has been claimed to directly modulate cloud formation (Svensmark and Friis-Christensen, 1997; Todd and Kniveton, 2001; Shaviv, 2002; Shaviv and Veizer, 2003; Kirkby, 2007; Svensmark et al., 2016; Svensmark, 2022). Changes in cloud cover directly induced by some kind of solar/astronomical forcings can have a significant impact on climate change because the clouds modify local and global albedos, resulting in more brightening or darkening periods (Scafetta, 2013a; Hofer et al., 2017; Pfeifroth et al., 2018; Pokrovsky, 2019), which could also easily alter the atmosphere–ocean circulation. Changes in UV irradiance are also known to have a chemical impact on the stratosphere by changing ozone concentration, and there might be many other mechanisms.

In general, changes in solar activity are expected to have a wide range of effects on the climate system because they alter the space weather conditions around the Earth (Moldwin, 2022). Several of these mechanisms are still poorly understood and others could still be unknown and, therefore, they cannot be incorporated into the present-day GCMs. Thus, the total climatic signature caused by changes in total solar activity (TSA), as opposed to that caused by TSI fluctuations alone, is what matters.

It is thus evident that the significant uncertainty regarding the real multi-decadal and secular changes in TSI, and the physical unknown regarding the broad array of Sun-climate mechanisms and their feedbacks imply that the GCMs are unlikely to accurately assess the overall climatic impact of solar activity changes by solely considering TSI radiative forcing, and even a specific one that was derived from two low-variability TSI proxy models.

Furthermore, changes in solar activity affect all climatic systems as well, including the greenhouse gas concentrations in the atmosphere. For example, the atmospheric concentration of CO_2 also varies because its solubility in the ocean depends on the sea surface temperature, which is also modulated by solar activity changes. However, the IPCC (Solomon et al., 2007; Stocker et al., 2014; Masson-Delmotte et al., 2021) assumed that, beside water vapor that is treated as a climatic feedback, all the other greenhouse gas variations and a variety of other climate factors that could have forced the climate system since 1750 are entirely anthropogenic. By doing so, it is possible to erroneously attribute some of the solar effect on the climate to humans. Some studies have even suggested that the frequency of earthquakes and volcanic eruptions slightly increases as solar activity decreases (Mazzarella and Palumbo, 1989; Stothers, 1989; Herdiwijaya et al., 2014; Bragato, 2015; Scafetta and Mazzarella, 2015). If this is the case, it may be necessary to take into account other types of geophysical feedbacks that could further magnify the effect of solar activity changes on the climate. Thus, several climatic forcings that the IPCC (Solomon et al., 2007; Stocker et al., 2014; Masson-Delmotte et al., 2021) assumed to be independent of solar activity changes could, instead, be partially influenced by the Sun itself, and such a portion, even if small, should be correctly attributed to solar activity changes.

The unresolved complexity of the physical problem requires empirical methodologies to assess the actual solar contribution to climate change. This has been typically attempted using a number of statistical tools such as cross-correlations, spectral filtering and coherence spectral and wavelet analysis, multi-linear regression analysis, and so on. When this is done, strong correlations and coherent patterns are often found between solar activity reconstructions and climate records covering time periods ranging from monthly to multi-millennial scales (Hoyt and Schatten, 1993, 1997; Cliver et al., 1998; Bond et al., 2001; Kerr, 2001; Neff et al., 2001; Fleitmann et al., 2003; Hu et al., 2003; Shaviv and Veizer, 2003; Scafetta et al., 2004; Scafetta and West, 2006; Kirkby, 2007; Eichler et al., 2009; Scafetta, 2009, 2011; Mufti and Shah, 2011; Steinhilber et al., 2012; Scafetta, 2013a; Soon and Legates, 2013; Vahrenholt and Lüning, 2013; Easterbrook, 2019; Miyahara et al., 2018; Connolly et al., 2021; Schmutz, 2021; Taricco et al., 2022; and many others).

The ACRIM-PMOD controversy on the long-term TSI trend from 1980 to 2000 also resulted in a disagreement regarding how much the change in solar activity contributed to the global surface warming between 1970 and 2000 (Scafetta and West, 2005, 2008, 2006;

Scafetta, 2009). According to PMOD, only anthropogenic activity could have caused such a warming. On the contrary, the increased trend of the ACRIM TSI satellite composite suggests that the Sun played a role in it, which raises the physical challenge of evaluating such a contribution (Scafetta and West, 2008).

In general, the PMOD TSI satellite composite implies (i) a small TSI multidecadal variability and the anthropogenic global warming hypothesis, and (ii) a strong climate sensitivity response to greenhouse gas variations and the physics already implemented in the present-day GCMs that predict alarming climate conditions for the near future. The ACRIM TSI composite, on the other hand, suggests (i) a larger TSI multidecadal and secular variability, and (ii) that the solar effect on climate needs to be carefully investigated in order to accurately assess the natural versus anthropogenic contributions to climate change. In the latter case, the anthropogenic contribution must be more moderate than what the GCMs claim.

Some researchers'public comments may even imply that the development of the PMOD TSI record and the IPCC's current endorsement of it are partially motivated by political concerns on the global warming issue. For example, Judith Lean (who in 1998 created the PMOD TSI composite together with Fröhlich) explained that "The fact that some people could use Willson's results (the ACRIM TSI composite) as an excuse to do nothing about greenhouse gas emissions is one reason we felt we needed to look at the data ourselves" (Lindsey, 2003). Also Zacharias (2014) demonstrated a similar political bias when concluded that: "A conclusive TSI time series is not only desirable from the perspective of the scientific community, but also when considering the rising interest of the public in questions related to climate change issues, thus preventing climate skeptics from taking advantage of these discrepancies within the TSI community by, e.g., putting forth a presumed solar effect as an excuse for inaction on anthropogenic warming".

In conclusion, Matthes et al. (2017) proposed that climate research should only use a solar forcing made with low secular-variability TSI proxy reconstructions (NRLTSI2 and the SATIRE) does not appear to be appropriate. Such proxy models do not represent the entire scientific literature on this topic and they implicitly assume correct the PMOD TSI composite, which is questionable. Several scientific teams have claimed that solar activity has changed significantly more (Hoyt and Schatten, 1993; Willson and Mordvinov, 2003; Shapiro et al., 2011; Egorova et al., 2018; Scafetta et al., 2019; Schmutz, 2021; Penza et al., 2022). Each TSI proxy model captures distinct aspects of observed changes in solar activity. All of them should be theoretically considered and all of them could be important for climate studies as well. In fact, Connolly et al. (2021) provided a broader overview of the ongoing debate on solar activity and its impact on climate change, arguing that the contribution of the Sun to climate change significantly depends on the solar and climatic records specifically used for the analysis.

Herein, in addition to the CMIP6 GCMs'specific low-variability TSI record, the most complementary, significant, and easily accessible TSI proxy models from 1700 to 2022 are also adopted. These models are characterized by low and high multi-decadal and secular variability (Fig. 2). I combine them to create three novel multi-proxy TSA records that, while not perfect, are expected to provide a more balanced assessment of the variations in solar activity reported in the scientific literature.

Lastly, I use a basic energy balance model calibrated using a differential multi-linear regression analysis to assess the effectiveness of the proposed TSA records in modeling a variety of global and ocean surface temperature records from 1850 to 2020, together with the anthropogenic and volcanic components. The proposed methodology is inspired by and improves on the author's past research (Scafetta and West, 2005, 2006; Scafetta, 2009) and on those of other researchers (e.g.: Soon et al., 2000; Lean and Rind, 2008, and others). A comparison with the TSI forcing function used by the CMIP6 GCMs is also examined.

2. Total solar irradiance proxy records

Three novel TSI proxy records from 1700 to 2022 were created using eight TSI records proposed in the academic literature (Fig. 2) that are commonly used also for climate change studies. Three records have low multidecadal variability (Krivova et al., 2007, 2010; Yeo et al., 2015; Coddington et al., 2016; Matthes et al., 2017) (Fig. 2A). One record was proposed 30 years ago by Hoyt and Schatten (1993) using specific solar constructors and presents a high multidecadal and secular variability. This TSI record was recently extended with the ACRIM TSI satellite composite (Fig. 2B) (Scafetta and Willson, 2014; Scafetta et al., 2019). Other four TSI records were proposed by Egorova et al. (2018), presenting a high multidecadal and secular variability (Fig. 2C). In the following, all records are rescaled to the ACRIM TSI satellite composite mean from 1981 to 2001. These two years represent the maxima of solar cycles 21 and 23. As a result, the TSI average from 1981 to 2001 is set to 1361.41 W/m^2 for all the following TSI records.

Matthes et al. (2017) developed their TSI model by merging NRLSSI2 (Coddington et al., 2016) and SATIRE (Krivova et al., 2010; Yeo et al., 2015) TSI models. The original TSI records range from 1700 to 2015, however, the record provided by Matthes et al. (2017) begins in 1850 like the CMIP6 GCM simulations. Thus, the TSI record representing the low multidecadal variability option and the PMOD TSI satellite composite is herein made of the TSI record by Matthes et al. (2017) linearly combined with the average of the other two records from 1700 to 1850. The three original TSI records are shown in Fig. 2A.

The TSI record representative of a high multidecadal variability with the ACRIM TSI composite is made of the original TSI proxy model by Hoyt and Schatten (1993) extended with the ACRIM TSI satellite composite (Willson and Mordvinov, 2003) from 1980 to 2012, the average between VIRGO-PMOD (Fröhlich, 2012) and SORCE-TIM (Kopp and Lean, 2011) TSI satellite records from 2013 to 2019, and between PMOD and TSIS (Richard et al., 2020; Coddington et al., 2021) records from 2020 to 2022. This TSI record is depicted in Fig. 2B and is provided in Supplementary Data Table S1 in the Supplement.

Averaging the four TSI reconstructions (PHI-US16, PHI-MU16, PHI-MC17, and SSR11) proposed by Egorova et al. (2018) provides the third TSI record representative of these other high multidecadal variability models. These data are based also on a combination of cosmogenic ^{10}Be and ^{14}C abundance records that are more directly connected with cosmic ray fluxes.

Fig. 3 compares the three proposed TSI average records discussed above. Several differences between them can be observed. In particular, the green curve presents a peak in the 1870s, which is not clearly observed in the other two curves; the red curve presents a peak in 1945–1950 while the blue curve peaks around 1960; the red curve also clearly increased from the 1970s to 2000, which is not clearly observed in the other two curves.

Fig. 4 depicts the three proposed "balanced" multi-proxy TSI reconstructions: model TSI #1 was made by averaging all three TSI records (blue, green and red curves) displayed in Fig. 3; model TSI #2 is made by averaging the green and red records; and model TSI #3 is made by averaging the blue and red records. These solar models are reported in Supplementary Data Tables S2, S3 and S4. From 1980 to 2020, the three TSI records displayed in Fig. 4 roughly replicate the trends of the Community-Consensus TSI satellite composite proposed by de Wit et al. (2017).

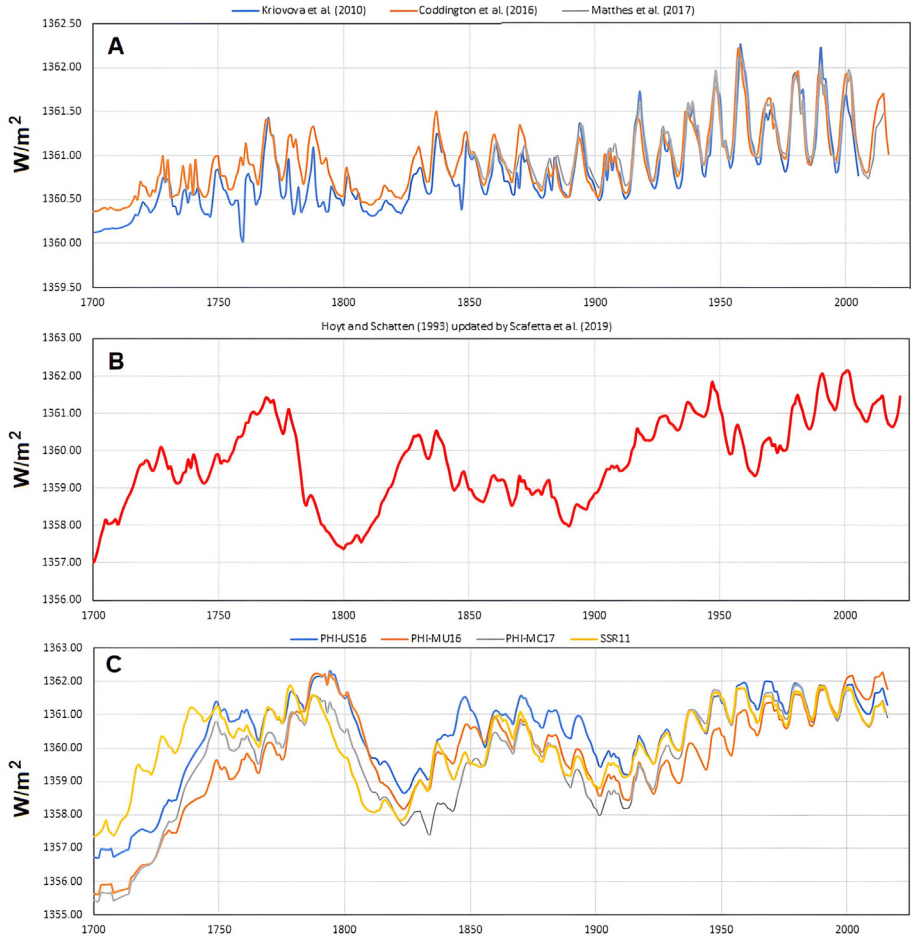

Fig. 2. TSI reconstructions: (A) Low multidecadal variability (after Krivova et al., 2010; Coddington et al., 2016; Matthes et al., 2017); (B) high multidecadal variability with ACRIM and other satellite TSI records since 1980 (Supplementary Data Table S1) (after Hoyt and Schatten, 1993; Scafetta et al., 2019); (C) high multidecadal variability (after Egorova et al., 2018).

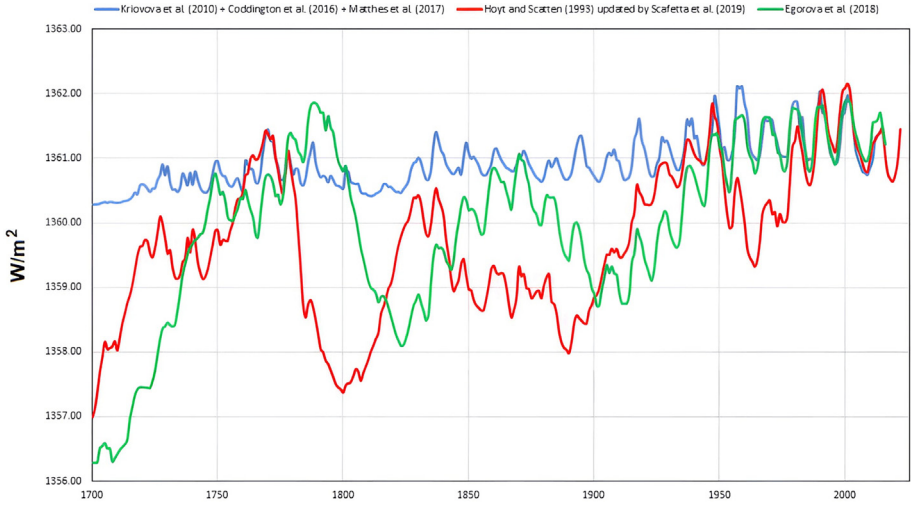

Fig. 3. Ensemble means of the TSI reconstructions with low (blue), high with ACRIM (red), and high (green) multidecadal variability shown in Fig. 2. (For interpretation of the references to colour in this figure legend, the reader is referred to the web version of this article.)

In the following sections, I hypothesize that the proposed TSI solar models also represent ideal TSA records, although still expressed in TSI units. Essentially, it is supposed that TSA can be represented by a function that is linearly related to the proposed TSI proxy functions.

3. The effective radiative forcing functions

Fig. 5A depicts the anthropogenic and volcanic effective radiative forcing functions used by the CMIP6 GCMs, which are reported in the Annex III of the IPCC-AR6 tables of historical and projected

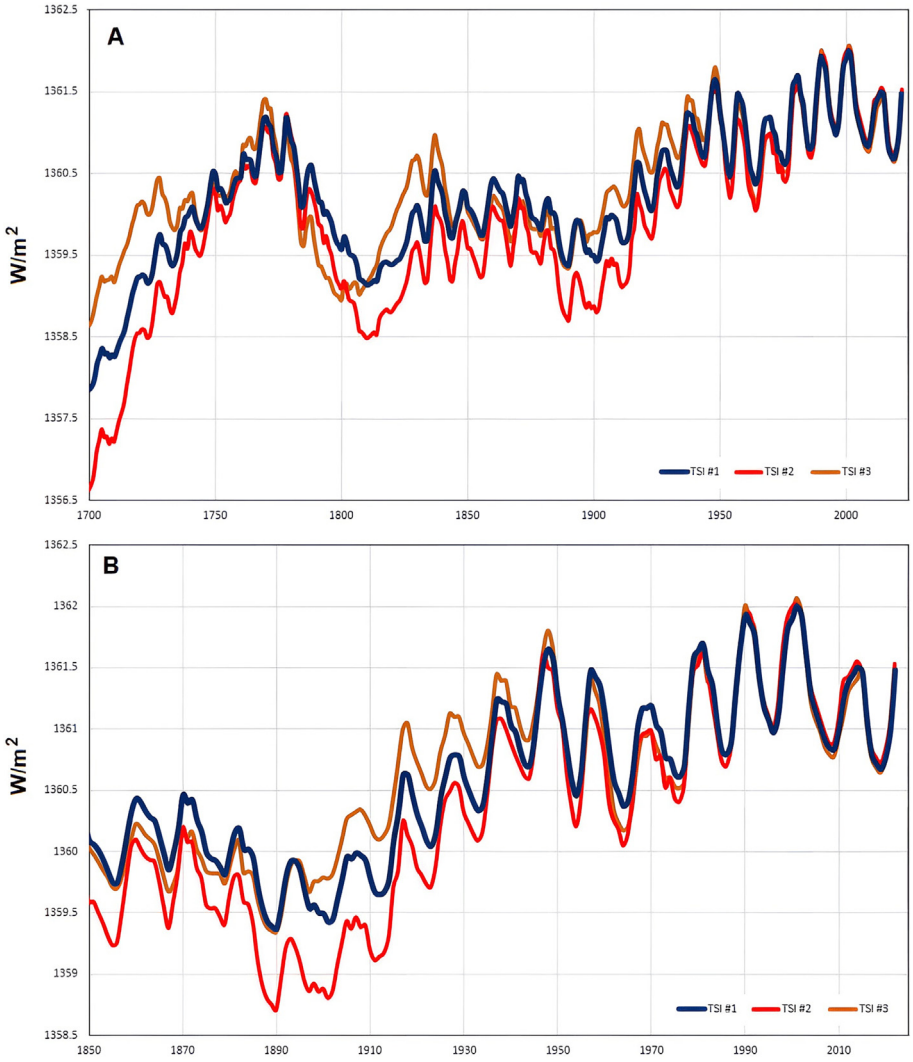

Fig. 4. (A) Balanced multi-proxy TSI reconstructions made of the TSI records shown in Fig. 3. TSI #1 averages the three TSI records; TSI #2 averages the green and red TSI records; TSI #3 averages the blue and green TSI records. (B) Zoom of Fig. 4A since 1850. These records are reported in Supplementary Data Tables S2, S3 and S4. (For interpretation of the references to colour in this figure legend, the reader is referred to the web version of this article.)

well-mixed greenhouse gas mixing ratios and effective radiative forcing of all climate forcing (Masson-Delmotte et al., 2021). These records are reported in Supplementary Data Table S5.

The solar effective radiative forcing function used by the CMIP6 GCMs is shown in Fig. 5B (green curve). Fig. 5B also depicts the three proposed balanced solar forcing functions derived from the TSI records shown in Fig. 4 (Supplementary Data Table S5). All records are scaled by the standard factor of 0.5/4 = 0.125, where 0.5 is the percentage of solar radiation that reaches the surface, which considers the mean albedo and the atmosphere's solar light absorption, and 4 is the ratio between the area of the Earth and that of the disk of the incoming solar radiation flux at the top of the atmosphere. All depicted TSI records range from 1850 to 2019 and are anomalies relative to their 1850 values.

The solar forcing functions depicted in Fig. 5B differ in several respects. Just a very modest secular trend can be seen for the solar forcing function used by the CMIP6 GCMs, which has remained nearly constant for about 200 years. Although not depicted in Fig. 5B, the TSI forcing adopted by the CMIP6 GCMs is so flat that even the 1790–1830 Dalton grand solar minimum almost coincides with the 1890–1910 solar minimum and the 2019 solar cycle minimum (Supplementary Data Table S5). Furthermore, because this record is also based on SATIRE and the PMOD TSI satellite composite, its solar effective forcing function decreased progressively from 1970 to 2020. Thus, by using this TSI record, the CMIP6 GCMs could only conclude that solar forcing did not account for almost any of the warming observed after the pre-industrial period (1850–1900), and, particularly, from 1980 to 2020 (Masson-Delmotte et al., 2021).

On the contrary, the other three TSI records reveal a multi-decadal oscillation as well as a clear increasing secular trend from the Dalton solar minimum to 2000. More specifically, they suggest that the TSI forcing significantly increased from the Dalton minimum (1810–1815) to around 1870–1876, then declined until around 1890–1905; it increased rapidly between 1910 and the 1940s, and declined again between 1950 and 1975. The TSI forcing then increased again until 2000, when it began to gradually fall until 2022. This oscillating pattern is especially noteworthy because, as demonstrated below, it is closely correlated with the changes observed in total surface temperature records, which show a very similar increasing trend and multi-decadal modulation (cf.: Scafetta et al., 2004; Scafetta and West, 2006, 2008; Scafetta, 2009; Scafetta, 2010, 2012b, 2013a, 2021b).

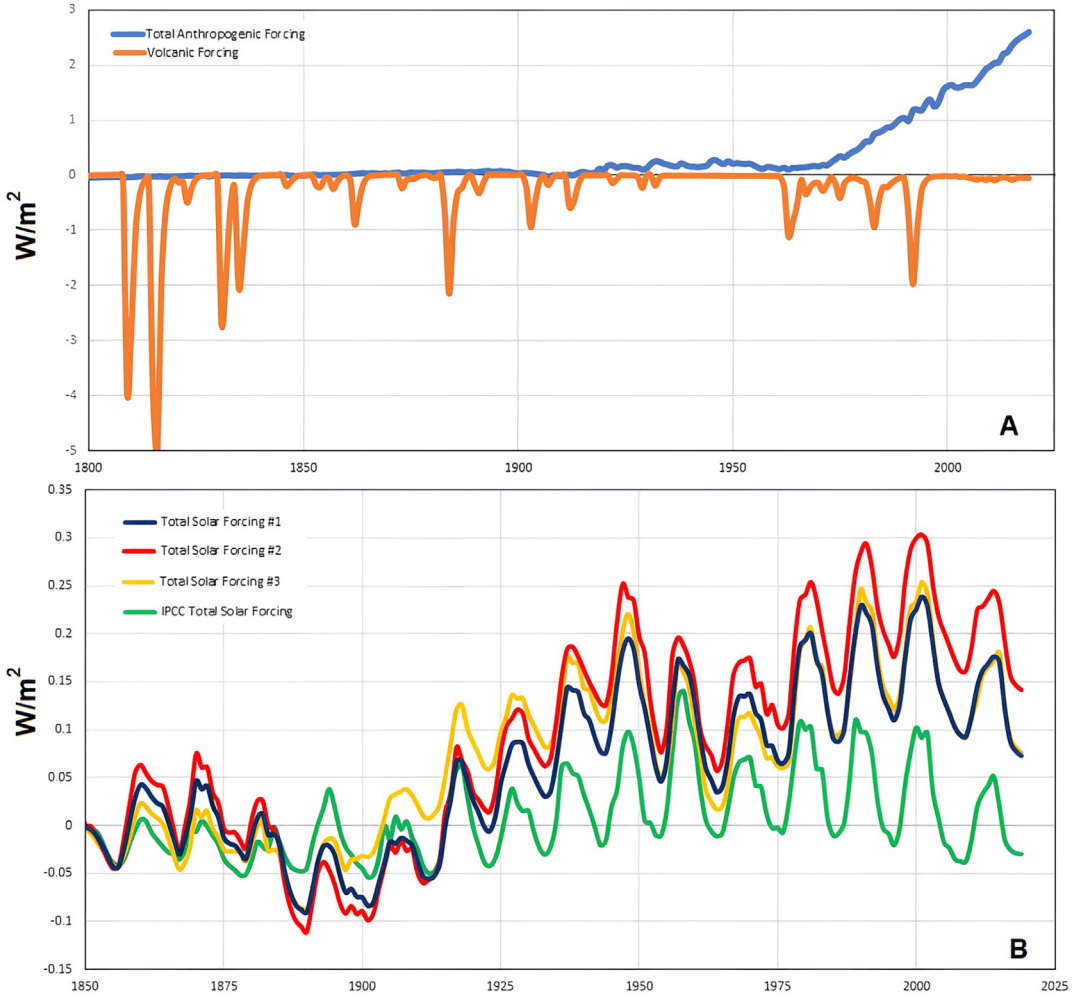

Fig. 5. (A) Anthropogenic (blue) and volcanic (orange) effective radiative forcing functions adopted by the CMIP6 GCMs (Masson-Delmotte et al., 2021). (B) Comparison between the solar effective radiative forcing function from Table Annex III of the IPCC-AR6 (green) (after Masson-Delmotte et al., 2021) and the three TSI forcing functions deduced from the TSI records shown in Fig. 4. All records are anomalies relative to their values in 1850. (For interpretation of the references to colour in this figure legend, the reader is referred to the web version of this article.)

4. Modeling global and sea surface temperature records

The global and sea surface temperature (SST) records are herein modeled by using a simple 1-D energy balance model (Scafetta, 2009). It is assumed that each temperature record, T (t), is made of three components — $T_A(t)$, $T_V(t)$, and $T_S(t)$ — generated by the anthropogenic, volcanic and solar forcings — $F_A(t)$, $F_V(t)$, and $F_S(t)$ — plus other fast fluctuations $\xi(t)$ (e.g., the ENSO), which are herein considered as random noise and are not reconstructed by the proposed model. For simplicity, the anthropogenic and volcanic forcings are supposed to be independent of the solar forcing, which, as discussed in the introduction, should slightly underestimate the solar contribution to climate changes.

Thus, T(t) is supposed to be given by the Eq. (1)

$$T(t) = T_A(t) + T_V(t) + T_S(t) + \xi(t) \tag{1}$$

All the above functions are supposed to be anomalies relative to t_0 = 1850, that is, it is assumed that $T(t_0)$ = 0 °C and $F(t_0)$ = 0 W/m^2. $T_A(t)$ is expected to be monotonically increasing, $T_V(t)$ is expected to be made of spikes that occasionally cool the climate for a few years (Thompson et al., 2009; Marshall et al., 2020), and $T_S(t)$ should presents a complex modulation that is also trending upward.

T(t) is supposed to vary in time according to the following differential Eq. (2)

$$\frac{dT(t)}{dt} = \frac{k[F(t) - F(0)] - [T(t) - T(0)]}{\tau}, \tag{2}$$

where F(t) the radiative forcing and τ is the characteristic time response of the system to a radiative perturbation. Eq. (2) assumes that the temperature and forcing functions are expressed as anomalies relative to given reference values, and the equation can be simplified by assuming T(0) = 0 °C and F(0) = 0 W/m^2.

The effective heat capacity of the system, which includes the ocean buffering effect, may be thought of as being represented by the system response time τ. The coefficient k represents the sensitivity of the system at equilibrium per unit of radiative forcing because, as Eq. (2) implies, for a step forcing increase equal to F(t) = 1 W/m^2 the temperature T(t) of the system must rise by k to reach the new thermal equilibrium.

Eq. (2) is herein used in its discrete form. Thus, for each forcing, the functions are computed with the Eqs. (3)–(5):

$$\frac{T_A(t) - T_A(t - \Delta t)}{\Delta t} = \frac{k_A F_A(t) - T_A(t - \Delta t)}{\tau} \tag{3}$$

$$\frac{T_V(t) - T_V(t - \Delta t)}{\Delta t} = \frac{k_V F_V(t) - T_V(t - \Delta t)}{\tau} \tag{4}$$

$$\frac{T_S(t)-T_S(t-\Delta t)}{\Delta t}=\frac{k_S F_S(t)-T_S(t-\Delta t)}{\tau} \quad (5)$$

The coefficients k_A, k_V and k_S are the climatic sensitivities associated with anthropogenic, volcanic and solar forcings, respectively. The characteristic time response τ is supposed to be the same for all forcings. It could also be noticed that the climate system could be characterized by several characteristic time responses (Scafetta, 2008, 2009), but herein this complication is ignored. Finally, Δt is the integration time interval.

The Eqs. (3), (4) and (5) describe, in first approximations, how the temperature of a system with a given heat capacity changes in time if externally perturbed by a given radiative forcing.

As anticipated, Eqs. (2) implies that a ΔF step increase causes the system to reach a new equilibrium temperature characterized by a change equal to $\Delta T = k\,\Delta F$. Thus, since a doubling of atmospheric CO_2 concentration from 280 ppm to 560 ppm amounts to a forcing of $\Delta F_{2\times CO_2} = 3.7$ W/m^2 (Rahmstorf, 2008), the quantity

$$\mathrm{ECS} = \Delta T_{2\times CO_2} = k_A\,\Delta F_{2\times CO_2} = 3.7\,k_A \quad (6)$$

is what is commonly defined as the "equilibrium climate sensitivity" (ECS). The alternative climate sensitive definition known as "transient climate response" (TCR) is given by the warming induces by increasing the atmospheric CO_2 concentration at 1% per year until it doubles. This means to calculate the warming induced by a radiative forcing function that linearly increases in time as $F(t) = 3.7\ t/70$ W/m^2 from t = 0 to t = 70 years, which can be easily calculated by integrating Eq. (3):

$$\mathrm{TCR} = 3.7\,k_A - \frac{3.7}{70}\,k_A\tau\left(1-e^{-70/\tau}\right) < \mathrm{ECS} \quad (7)$$

TCR is smaller than ECS due to its "transient" nature. Below I discuss two ways of doing the calculations.

4.1. Case 1: Anthropogenic, volcanic and solar forcings are radiative forcings alone

The anthropogenic, volcanic, and solar forcings can be assumed to be physically equivalent, implying that the climate system responds to them in the same way as radiative forcings. GCMs process climate forcings in this manner because all forcings are supposed to be radiative. Thus, $k_{AVS} = k_A = k_V = k_S$ and Eq. (2) can be directly used as

$$\Theta(t)=\frac{T(t)-T(t-\Delta t)}{\Delta t}=\frac{k_{AVS}F_{AVS}(t)-T(t-\Delta t)}{\tau} = \alpha_{AVS}F_{AVS}(t)-\beta\,T(t-\Delta t) \quad (8)$$

where $\alpha_{AVS} = k_{AVS}/\tau$, $\beta = 1/\tau$, and $\Delta t = 1$ year. The two regression parameters of Eq. (8), α_{AVS} and β, can be calculated using a multilinear regression algorithm because the functions $\Theta(t)$, $T(t)$, and $F_{AVS}(t) = F_A(t) + F_V(t) + F_{TSI}(t)$ are known.

Finally, the temperature signature induced by the total forcing can be calculated by integrating the equation

$$T_{AVS}(t) = T_{AVS}(t-\Delta t) + [\alpha_{AVS}\,F_{AVS}(t) - \beta\,T_{AVS}(t-\Delta t)]\Delta t \quad (9)$$

The ECS predicted by the model is $3.7\ k_A = 3.7\ \alpha_{AVS}/\beta$.

4.2. Case 2: Solar forcing physically differs from anthropogenic and volcanic radiative forcings

The climate's response to TSA changes includes, but it likely does not equal, that to TSI changes alone. In fact, as mentioned in the Introduction, TSI forcing is likely only one of the solar mechanisms influencing the climate of the Earth. Changes in solar activity could affect the climate system through several correlated mechanisms, including TSI forcing, UV forcing, cosmic ray forcing, solar wind forcing, other magnetic and solar-related interplanetary corpuscular forcings, and others. As a result, changes in TSA may have a far stronger overall impact on the climate than the TSI forcing alone. A realistic GCM should account for all Sun-climate interactions to properly assess the real role of the Sun in climate change.

In this scenario, the proposed TSI proxy forcing functions are viewed as generalized TSA functions. Thus, the solar input function is no longer an actual radiative forcing but rather a function that represents TSA, albeit it is still represented in radiative units. Eq. (5) automatically considers the TSI functions as TSA proxies when k_S is allowed to differ from the climate sensitivities, $k_A = k_V$, to the anthropogenic and volcanic radiative forcings.

More specifically, it is assumed that

$$F_{TSA} = F_{TSI} + F_{other\ solar\ forcings} = F_{TSI} + c\,F_{TSI} = (1+c)F_{TSI} \quad (10)$$

where c is a constant. Consequently, by using in Eq. (5), $F_S = (1 + c)\,F_{TSI}$, I get $k_S = (1 + c)\,k_{AV} \propto k_{AV}$, where $k_{AV} = k_A = k_V$ is the sensitivity to the radiative forcing alone.

Thus, the Eqs. (3)–(5) can be combined as Eq. (11)

$$\Theta(t)=\frac{T(t)-T(t-\Delta t)}{\Delta t} = \frac{k_{AV}F_{AV}(t)-T_{AV}(t-\Delta t)}{\tau}+\frac{k_S F_{TSI}(t)-T_S(t-\Delta t)}{\tau} \quad (11)$$

where the AV component evaluates the role played by anthropogenic and volcanic radiative forcing, while the S component evaluates the role played by the TSA changes.

Eq. (11) can be rewritten as Eq. (12)

$$\Theta(t) = \alpha_{AV}F_{AV}(t) + \alpha_S F_{TSI}(t) - \beta\,T(t-\Delta t) \quad (12)$$

where $F_{AV}(t) = F_A(t) + F_V(t)$. The three free parameters $\alpha_{AV} = k_{AV}/\tau$, $\alpha_S = k_S/\tau$, and $\beta = 1/\tau$ of Eq. (12) can be evaluated by using a multi-linear regression algorithm because the functions $\Theta(t)$, $T(t)$, $F_{AV}(t)$, and $F_{TSI}(t)$ are known. In this case, $\alpha_{AV} = \alpha_A = \alpha_V \neq \alpha_S$ and $k_{AV} = k_A = k_V \neq k_S$.

Once the regression coefficients are determined, $T_A(t)$, $T_V(t)$, and $T_S(t)$ can be evaluated by recurrent integrations as

$$T_A(t) = T_A(t-\Delta t) + [\alpha_{AV}F_A(t) - \beta\,T_A(t-\Delta t)]\Delta t \quad (13)$$

$$T_V(t) = T_V(t-\Delta t) + [\alpha_{AV}F_V(t) - \beta\,T_V(t-\Delta t)]\Delta t \quad (14)$$

$$T_S(t) = T_S(t-\Delta t) + [\alpha_S F_{TSI}(t) - \beta\,T_S(t-\Delta t)]\Delta t \quad (15)$$

where $\Delta t = 1$ year is the integration time-step. The temperature signature induced by the three components is

$$T_{AVS}(t) = T_A(t) + T_V(t) + T_S(t). \quad (16)$$

The model ECS is $3.7\ \alpha_{AV}/\beta$ because it is defined as a function of radiative forcing alone. However, it is also possible to define the quantity $3.7\ \alpha_S/\beta$ that must be interpreted as a form of "proxy" ECS because it is relative to TSA changes albeit given in TSI proxy units. As a result, the ratio α_S/α_{AV} illustrates how much greater influence the TSA input has on the climate than just the TSI effect alone.

4.3. Comments

Eq. (12) might be extended further by separating the volcanic and anthropogenic forcings, but it is unclear why the climate sensitivity should differ between them. Consequently, k_A and k_V can be treated as equal.

It should be again noted that a portion of $F_{AV}(t)$ could be a feedback to the solar forcing $F_S(t)$. Thus, the solar signature obtained from the proposed multi-linear regression algorithm may partially underestimate the true solar effect on the climate because a por-

tion of the solar signature could be embedded inside $T_{AV}(t) = T_A(t) + T_V(t)$. Connolly et al. (2021) attempted to account for this partial dependency of the anthropogenic and volcanic forcings on the solar forcing by fitting the temperature records with the solar record first, rather than using a simultaneous regression of the solar and anthropogenic/volcanic components, as done here. However, their methodology could be problematic because of the collinearity, although modest, between the solar and anthropogenic constructors since they both trend up from 1900 to 2020. Thus, their algorithm would maximize the solar contribution relative to the anthropogenic one and, thus, overestimating it.

Actually, this limitation was explicitly acknowledged by Connolly et al. (2021) on page 52 of their paper and was later also highlighted in Richardson and Benestad (2022)'s critique. Scafetta (2013b) demonstrated that the collinearity problem between the solar and anthropogenic forcings can only be solved by analyzing at least 1000-year-long temperature records (from the Medieval Warm Period to the Current Warm Period) because both solar and temperature records show a millennial cycle that is not present in the anthropogenic forcing record. By using such a methodology, Scafetta (2013b) showed that about half of the warming from 1900 to 2020 could be associated with solar activity changes using the proxy temperature model proposed by Moberg et al. (2005) and the available global surface temperature records since 1850.

The above complexities are here ignored, and the two constructors, $F_{AV}(t)$ and $F_S(t)$, are assumed to be physically and geometrically sufficiently independent of each other and are processed concurrently by the multi-linear regression algorithm, although, as previously explained, in this way the solar effect may still be partially underestimated because a portion of $F_{AV}(t)$ could be physically generated by TSA changes.

The proposed methodology upgrades previous works by the author (Scafetta and West, 2005, 2006; Scafetta, 2009) and adopts differential multilinear regression algorithms (Eqs. (8) and (12) by taking into account that the forcing functions should be processed by some kind of climate model, even a very simple one as Eq. (2) proposes, before they can be used as temperature constructors in a multi-regression algorithm. In fact, one of the regression coefficients, $\beta = 1/\tau$, is related to the characteristic time response of the climate system, which is a dynamical feature of the system. Thus, the proposed methodology corrects the simplistic multi-regression methodologies used in other studies (Douglass and Clader, 2002; Gleisner and Thejll, 2003; Connolly et al., 2021; Richardson and Benestad, 2022), in which the radiative forcing functions themselves, or even their generating functions, are erroneously considered to represent direct regression constructors of the temperature record. In fact, if the forcing functions are not linearly related to their temperature signatures, any linear superposition of them is physically inappropriate, or, at least not optimal, for representing their associated temperature changes.

5. Results

The hindcasts of the multi-linear regression analysis using Eqs. (8) and (12) are shown in Figs. 6 and 7, and reported in Table 1. The procedure is repeated for four climatic records: two global surface temperature records HadCRUT4 (Morice et al., 2012) and HadCRUT5 (non-infilled data) (Morice et al., 2021), and two global sea surface temperature records HadSST3 (Kennedy et al., 2011a, b) and HadSST4 (Kennedy et al., 2019) (Supplementary Data Table S6). The latter are used also because the land records could be significantly affected by non-climatic warm biases due, for example, to insufficiently corrected urban heat island (UHI) trends (Connolly et al., 2021; Scafetta, 2021a, 2023a,b); thus, the SST records could provide an alternative evaluation of the sensitivities.

5.1. CMIP6 GCMs radiative forcings

The first line of Figs. 6 and 7 show the results of Eq. (8) with the anthropogenic, volcanic, and solar forcing functions employed in the CMIP6 GCMs. If the Sun only acts on the climate system through the TSI changes proposed by Matthes et al. (2017), nearly all of the warming observed from 1850 to 1900 to 2020 is due to anthropogenic forcing because the solar contribution to the observed global and sea surface temperature records is extremely small. In fact, the Sun could have contributed only about 2%–3% of the warming from 1850–1900 to 2010–2019. This is also what the IPCC advocates (Solomon et al., 2007; Stocker et al.., 2014; Masson-Delmotte et al., 2021).

The analysis made using the global surface temperature records, HadCRUT4 (Morice et al., 2012) and HadCRUT5 (Morice et al., 2021), suggest that the likely value of the actual ECS could be between 1.4 °C and 2.8 °C with a mean of 2.1 °C, which roughly corresponds to what has been found in other studies (Lewis and Curry, 2018; Scafetta, 2021c, 2022, 2023a, 2022; Lewis, 2023) and would agree with the CMIP6 GCMs that predict an ECS between 1.8 °C and 3.0 °C. The calculations made using HadSST3 (Kennedy et al., 2011a,b) and HadSST4 (Kennedy et al., 2019) suggest an ECS value between 1.1 °C and 2.4 °C with an average of 1.75 °C.

The panels on the first line of Figs. 6 and 7 also show that the modeled temperature $T_{AVS}(t)$ reconstructs less than half of the warming observed from 1900 to 1945, which was nearly as strong as that observed between 1970 and 2000 (Scafetta, 2010, 2013a; Loehle, 2014), despite the relatively low anthropogenic forcing present in the first half of the 20th century. Indeed, the warming from 1900 to 1950 is poorly reproduced by the GCMs (Scafetta, 2012b, 2013a), implying that these models either used an incorrect solar forcing function or are unable to reproduce an important quasi 60-year natural oscillation of the climate system (Scafetta, 2010, 2012b, 2013a, 2013c; Loehle and Scafetta, 2011; Wyatt and Curry, 2013; Loehle, 2014).

Although herein not shown in any figure or table, the same analysis was repeated by substituting the GCM-adopted TSI forcing with the three balanced TSI records. The solar effect was found to be approximately 3–4 times larger than in the former case, while the anthropogenic contribution diminished by about 10%. Using the global surface records, the ECS lowered a little bit, and was estimated to be 1.85 ± 0.6 °C. ECS was estimated to be 1.55 ± 0.6 °C using the sea surface temperature records. By adopting the new proposed TSI records showing a larger secular variability (Figs. 4 and 5B), if the Sun influences the climate system through TSI changes alone, it could have been responsible for roughly 10%, or less, of the warming from 1850–1900 to 2010–2019. Thus, substituting the TSI forcing of the GCMs with the new ones would only slightly mitigate the IPCC's conclusion that nearly all warming observed from 1850 to 2020 was caused by human activity. However, only the CMIP6 GCMs with the lowest ECS would still be compatible with the data according to the proposed modelling.

5.2. CMIP6 GCMs radiative forcings and additional solar effects

The second line of Figs. 6 and 7 shows the results obtained with Eq. (12) processed with the anthropogenic, volcanic, and solar forcing functions used by the CMIP6 GCMs. In this second scenario, the solar forcing function is supposed to be a proxy for TSA changes. Thus, it is assumed that the climate sensitivity k_S can differ from the climate sensitivity to radiative forcing alone, which is given by $k_{AV} = k_A = k_V$.

The climatic signature of the anthropogenic forcing was found to be 5%–15% smaller than in the scenario investigated in Section 5.1, whereas the solar signature was found to be substantially bigger. k_S was found to be 4.3 ± 2.5 and 5.0 ± 3.0 times greater than

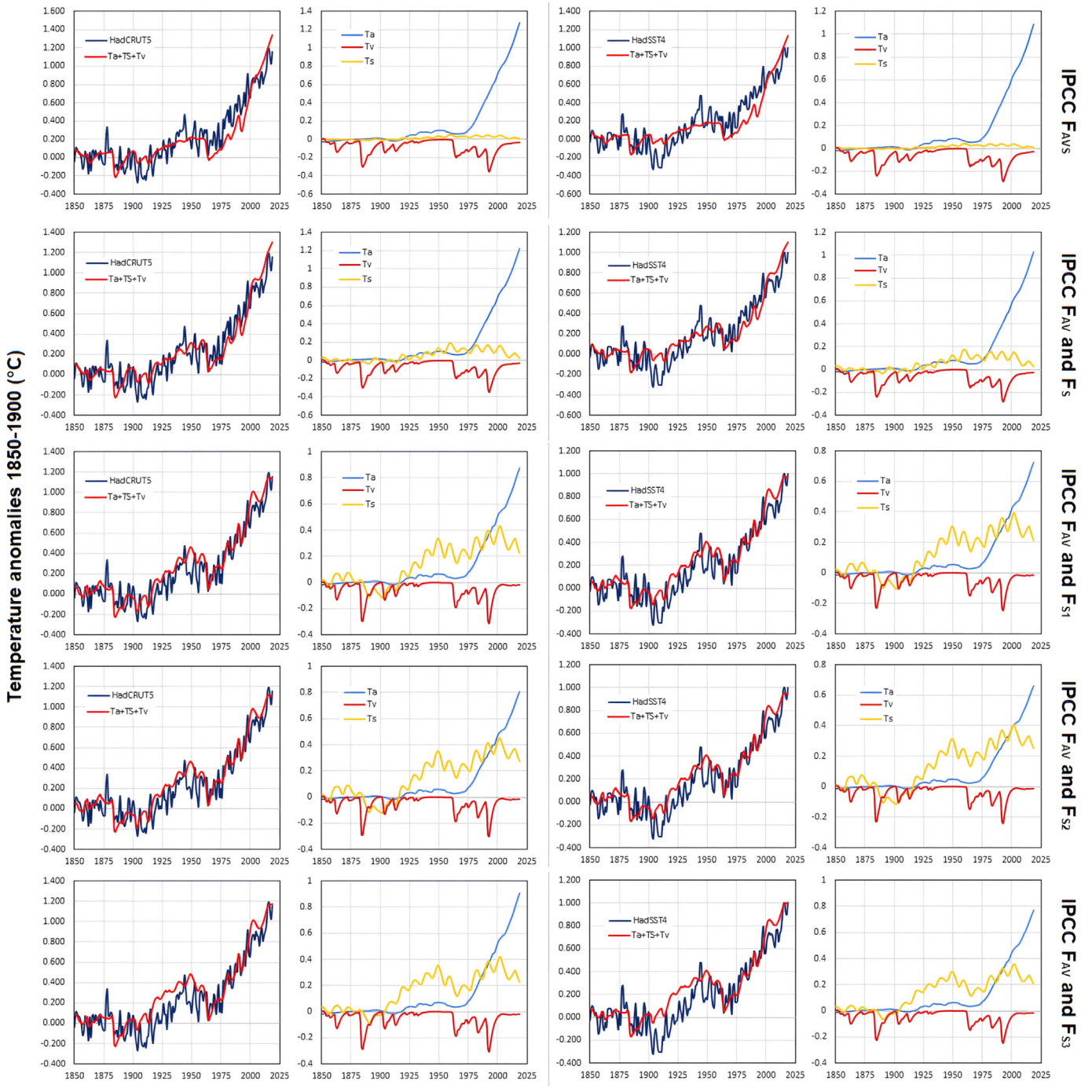

Fig. 6. Analysis of HadCRUT5 (after Morice et al., 2021) (right) and HadSST4 (Kennedy et al., 2019) (left): (line-1) using Eq. (9) and the CMIP6 GCMs forcings; (lines 2–5) using Eq. (12) and the anthropogenic and volcano forcing of the CMIP6 GCMs forcings and the three solar forcing functions depicted in Fig. 5B.

k_{AV} using the global and sea surface temperature records, respectively.

This result suggests that most of the Sun's influence on the climate could be caused by mechanisms complementary to the TSI forcing alone. This also implies that, by assuming that the Sun's role is limited to TSI radiative forcing alone, the GCMs are expected to drastically underestimate the solar effect on climate change.

In such a scenario, the ECS was found to be a little bit lower than determined in Section 5.1: 1.95 ± 0.6 °C for HadCRUT4 and HadCRUT5, and 1.6 ± 0.6 °C for HadSST3 and HadSST4. Thus, also in this case, the solar climatic signature would be still modest relative to the anthropogenic one, as the figures show. However, only the CMIP6 GCMs with the lowest ECS would be compatible with the data.

5.3. CMIP6 GCMs anthropogenic and volcano forcings, the three "balanced" TSI records and additional solar effects

The panels in the third, fourth, and fifth lines of Figs. 6 and 7 show the results of Eq. (12) with the three balanced TSI records depicted in Fig. 4B, together with the anthropogenic and volcanic effective forcing functions used by the CMIP6 GCMs.

In this scenario, the solar contribution to climate change is found to be substantially larger than in the cases analyzed in Sec-

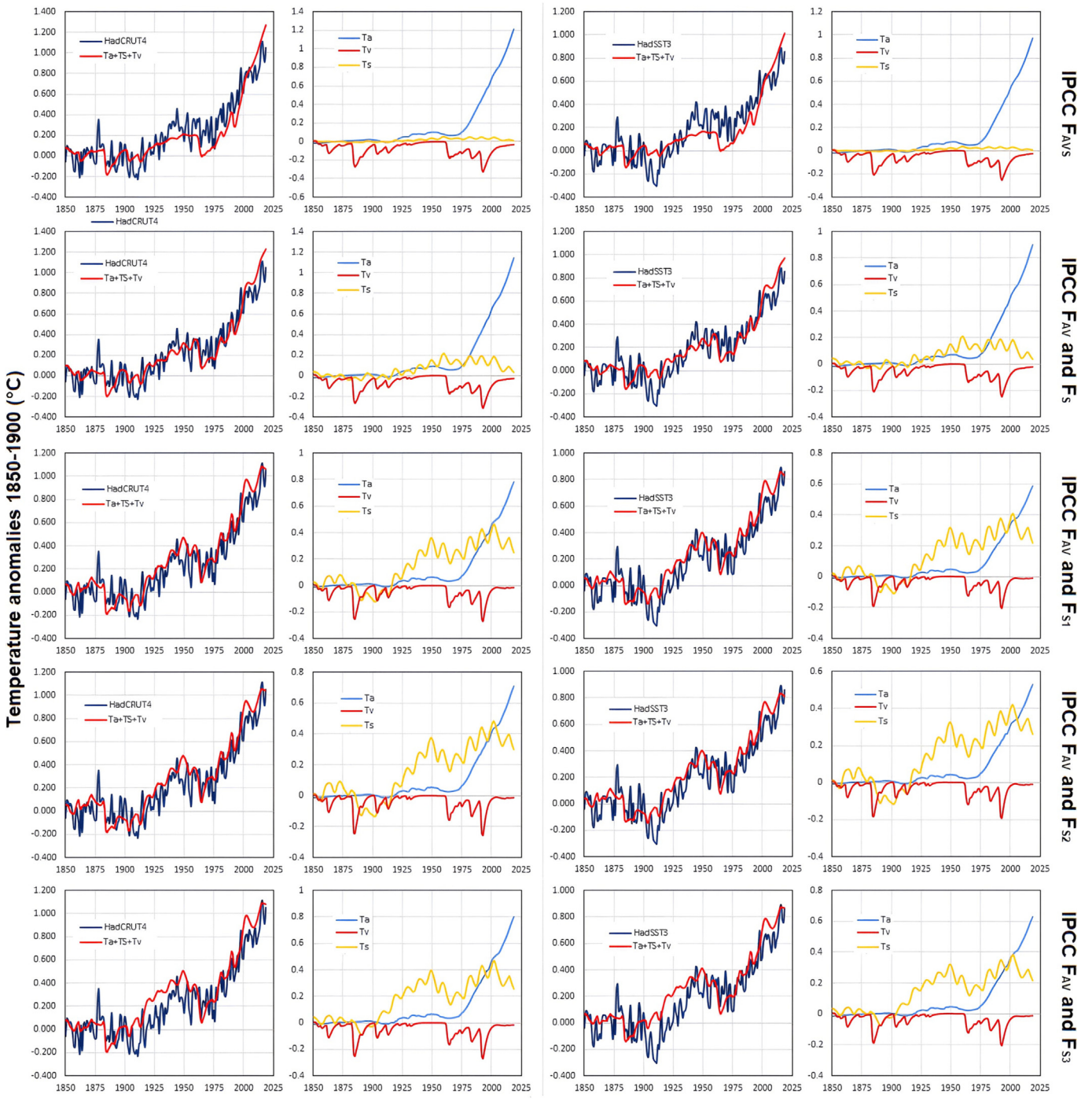

Fig. 7. Analysis of HadCRUT4 (Morice et al., 2012) (right) and HadSST3 (Kennedy et al., 2011a,b) (left): (line-1) using Eq. (9) and the CMIP6 GCMs forcings; (lines 2–5) using Eq. (12) and the anthropogenic and volcano forcing of the CMIP6 GCMs forcings and the three solar forcing functions depicted in Fig. 5B.

tions 5.1 and 5.2. Furthermore, the proposed TSI input functions provide temperature signatures that more closely match the surface temperature records: see the values reported in the correlation line in Table 1.

The solar and climatic records show a consistently increasing trend and a virtually synchronous multidecadal modulation. Both functions approximately rise from 1850 to 1880, decline from 1880 to 1905, considerable increase from 1910 to the 1940s, moderately decline from 1950 to 1975, and again increase from 1980 to 2000. Between 2000 and 2014, anthropogenic warming appears to have been offset by the cooling caused by the 11-year solar cycle minimum. The peak of solar cycle 24, which occurred between 2012 and 2014, appears to have contributed to the temperature rise between 2015 and 2020, together with some anthropogenic warming. This temperature rise was further stressed by two strong El-Niño events, as better shown in Fig. 8B and 8B'. In fact, the estimated time response τ is 3–4 years. This suggests that the minimum between solar cycles 24 and 25 (which occurred in December 2019), may have been responsible for the slight global cooling observed from 2016 to 2022. Scafetta (2021b) showed a similar result using a harmonic model of the global surface temperature record.

Table 1
Evaluation of the multilinear regression parameters of Eqs. (8) and (12). The "IPCC Forcings" column assumes Eq. (8) and the total effective forcing $F_{AVS}(t) = F_A(t) + F_V(t) + F_S(t)$ as provided by the IPCC (after Masson-Delmotte et al., 2021). The other four columns assume Eq. (12), the effective forcing $F_{AV}(t) = F_A(t) + F_V(t)$ as provided by the IPCC (after Masson-Delmotte et al., 2021), and the four effective solar forcings depicted in Fig. 5B. The characteristic time response of the system is $\tau = 1/\beta$. ECS is 3.7 k_A = 3.7 α_A/β and 3.7 k_S = 3.7 α_S/β is the "proxy" equilibrium climate sensitivity to solar activity changes relative to the adopted TSI proxy; TCR values are calculated using Eq. (7). Finally, the coefficient of correlation between the temperature record and the modeled temperature record, $T_{AVS}(t) = T_A(t) + T_V(t) + T_S(t)$, is given by corr.

			IPCC Forcings	TSI_{IPCC}	TSI_1	TSI_2	TSI_3
HadCRUT5	α_{AVS}	°C/(Wm^{-2} yr)	0.093 ± 0.020	–	–	–	–
	α_{AV}	°C/(Wm^{-2} yr)	–	0.094 ± 0.020	0.107 ± 0.019	0.110 ± 0.019	0.103 ± 0.019
	α_S	°C/(Wm^{-2} yr)	–	0.365 ± 0.198	0.570 ± 0.134	0.514 ± 0.108	0.473 ± 0.119
	β	1/yr	0.163 ± 0.037	0.174 ± 0.038	0.293 ± 0.048	0.331 ± 0.051	0.269 ± 0.046
	$\tau = 1/\beta$	yr	6.1 ± 1.4	5.7 ± 1.3	3.4 ± 0.6	3.0 ± 0.5	3.7 ± 0.6
	ECS = 3.7 k_A	°C	2.1 ± 0.7	2.0 ± 0.6	1.4 ± 0.3	1.2 ± 0.3	1.4 ± 0.4
	TCR = Eq. (7)	°C	1.9 ± 0.6	1.8 ± 0.5	1.3 ± 0.3	1.2 ± 0.3	1.3 ± 0.3
	3.7 k_S	°C	2.1 ± 0.7	7.8 ± 4.5	7.2 ± 2.1	5.8 ± 1.5	6.5 ± 2.0
	k_S/k_A	–	1	3.9 ± 2.3	5.3 ± 1.6	4.7 ± 1.3	4.6 ± 1.4
	corr.	–	0.91	0.93	0.95	0.95	0.93
HadSST4	$\alpha_{AV\ S}$	°C/(Wm^{-2} yr)	0.073 ± 0.017	–	–	–	–
	α_{AV}	°C/(Wm^{-2} yr)	–	0.074 ± 0.017	0.083 ± 0.016	0.083 ± 0.016	0.076 ± 0.016
	α_S	°C/(Wm^{-2} yr)	–	0.316 ± 0.174	0.482 ± 0.117	0.427 ± 0.094	0.350 ± 0.101
	β	1/yr	0.147 ± 0.036	0.160 ± 0.037	0.272 ± 0.047	0.303 ± 0.050	0.229 ± 0.044
	$\tau = 1/\beta$	yr	6.8 ± 1.7	6.3 ± 1.4	3.7 ± 0.6	3.3 ± 0.5	4.4 ± 0.8
	ECS = 3.7 k_A	°C	1.8 ± 0.6	1.7 ± 0.6	1.1 ± 0.3	1.0 ± 0.3	1.2 ± 0.4
	TCR = Eq. (7)	°C	1.7 ± 0.5	1.6 ± 0.5	1.1 ± 0.3	1.0 ± 0.2	1.2 ± 0.3
	3.7 k_S	°C	1.8 ± 0.6	7.3 ± 4.4	6.6 ± 2.0	5.2 ± 1.4	5.7 ± 2.0
	k_S/k_A	–	1	4.3 ± 2.5	5.8 ± 1.8	5.1 ± 1.5	4.6 ± 1.6
	corr.	–	0.89	0.91	0.94	0.94	0.91
HadCRUT4	α_{AVS}	°C/(Wm^{-2} yr)	0.081 ± 0.019	–	–	–	–
	α_{AV}	°C/(Wm^{-2} yr)	–	0.082 ± 0.018	0.090 ± 0.018	0.091 ± 0.018	0.089 ± 0.018
	α_S	°C/(Wm^{-2} yr)	–	0.385 ± 0.200	0.571 ± 0.137	0.517 ± 0.112	0.518 ± 0.125
	β	1/yr	0.145 ± 0.036	0.158 ± 0.036	0.273 ± 0.047	0.310 ± 0.050	0.264 ± 0.045
	$\tau = 1/\beta$	yr	6.9 ± 1.7	6.3 ± 1.4	3.7 ± 0.6	3.2 ± 0.5	3.8 ± 0.6
	ECS = 3.7 k_A	°C	2.1 ± 0.7	1.9 ± 0.6	1.2 ± 0.3	1.1 ± 0.3	1.2 ± 0.3
	TCR = Eq. (7)	°C	1.9 ± 0.6	1.7 ± 0.5	1.2 ± 0.3	1.0 ± 0.3	1.2 ± 0.3
	3.7 k_S	°C	2.1 ± 0.7	9.0 ± 5.1	7.7 ± 2.3	6.2 ± 1.7	7.3 ± 2.1
	k_S/k_A	–	1	4.7 ± 2.6	6.3 ± 2.0	5.7 ± 1.7	5.8 ± 1.8
	corr.	–	0.90	0.93	0.94	0.94	0.92
HadSST3	α_{AVS}	°C/(Wm^{-2} yr)	0.063 ± 0.015	–	–	–	–
	α_{AV}	°C/(Wm^{-2} yr)	–	0.065 ± 0.015	0.068 ± 0.014	0.066 ± 0.014	0.064 ± 0.015
	α_S	°C/(Wm^{-2} yr)	–	0.369 ± 0.173	0.508 ± 0.118	0.446 ± 0.095	0.389 ± 0.103
	β	1/yr	0.141 ± 0.036	0.159 ± 0.037	0.276 ± 0.047	0.307 ± 0.050	0.238 ± 0.044
	$\tau = 1/\beta$	yr	7.1 ± 1.8	6.3 ± 1.5	3.6 ± 0.6	3.3 ± 0.5	4.2 ± 0.8
	ECS = 3.7 k_A	°C	1.7 ± 0.6	1.5 ± 0.5	0.9 ± 0.3	0.8 ± 0.2	1.0 ± 0.3
	TCR = Eq. (7)	°C	1.5 ± 0.5	1.4 ± 0.4	0.9 ± 0.2	0.8 ± 0.2	0.9 ± 0.3
	3.7 k_S	°C	1.7 ± 0.6	8.6 ± 4.5	6.8 ± 2.0	5.4 ± 1.4	6.0 ± 2.0
	k_S/k_A	–	1	5.7 ± 3.0	7.5 ± 2.3	6.8 ± 2.0	6.1 ± 2.1
	corr.	–	0.86	0.91	0.92	0.92	0.89

Table 1 also reports the Pearson correlation coefficients between the actual temperature records and the modeled temperature records, $T_{AVS}(t) = T_A(t) + T_V(t) + T_S(t)$. The highest correlation coefficients are found for the TSI proxy models #1 and #2, indicating that the Matthes et al. (2017) low secular-variability TSI record, which was used in the CMIP6 GCMs and whose weight is larger in the TSI proxy model #3, could be a rather poor choice for reconstructing the multi-decadal climatic patterns seen in the global and sea surface temperature records.

Fig. 8 compares the HadCRUT5 global surface temperature record to (A) the CMIP6 GCM ensemble mean record and (B) the energy balance model (Eq. (16)) using the proposed TSI proxy model #2, which does not use the GCMs' low secular-variability TSI record. The GCM simulation depicted in Fig. 8A monotonically warms up, although occasional volcanic eruptions momentarily cause cold spikes; the monotonic warming trend produced by the model is simulated by the green curve. On the contrary, the model provided in Fig. 8B indicates an oscillating pattern developing around a warming trend. The global surface temperature record shows a similar growing trend, regulated by an approximately 60-year oscillation: the period 1880–1910 experienced a global cooling; the period 1910–1940 was characterized by considerable warming; and the period 1940–1970 experienced another global cooling. From 1880 to 1970, the model in Fig. 8B reproduces this oscillating pattern more precisely (corr. coeff. r = 0.79) than the CMIP6 GCM ensemble average simulation depicted in Fig. 8A (corr. coeff. r = 0.74). Thus, Fig. 8 illustrates that the suggested model (red curve, Fig. 8B) exhibits a multidecadal modulation that correlates significantly better with the temperature record (blue curve) than the GCM ensemble average simulation (red curve, Fig. 8A).

The different performance of the CMIP6 GCM ensemble average simulation and of the proposed regression model in reproducing the temperature pattern from 1850 to 1950 becomes more evident if a quadratic upward trend is detrended from the records. The correlation coefficient is r = 0.45 using the GCM ensemble average simulation (Fig. 8A'), and r = 0.55 using the proposed regression model (Fig. 8B'). This result suggests that the observed multidecadal modulation of the temperature records could have been mostly determined by solar forcings, and not by chaotic internal oscillations of the climate system.

Additionally, also from 2000 to 2020 the model indicated by the red curve in Fig. 8B reproduces the temperature record more closely than the GCM red curve in Fig. 8A. In fact, Fig. 8A shows that the CMIP6 GCM simulation rapidly warms up, whereas Fig. 8B shows that the modeled temperature presents a standstill between

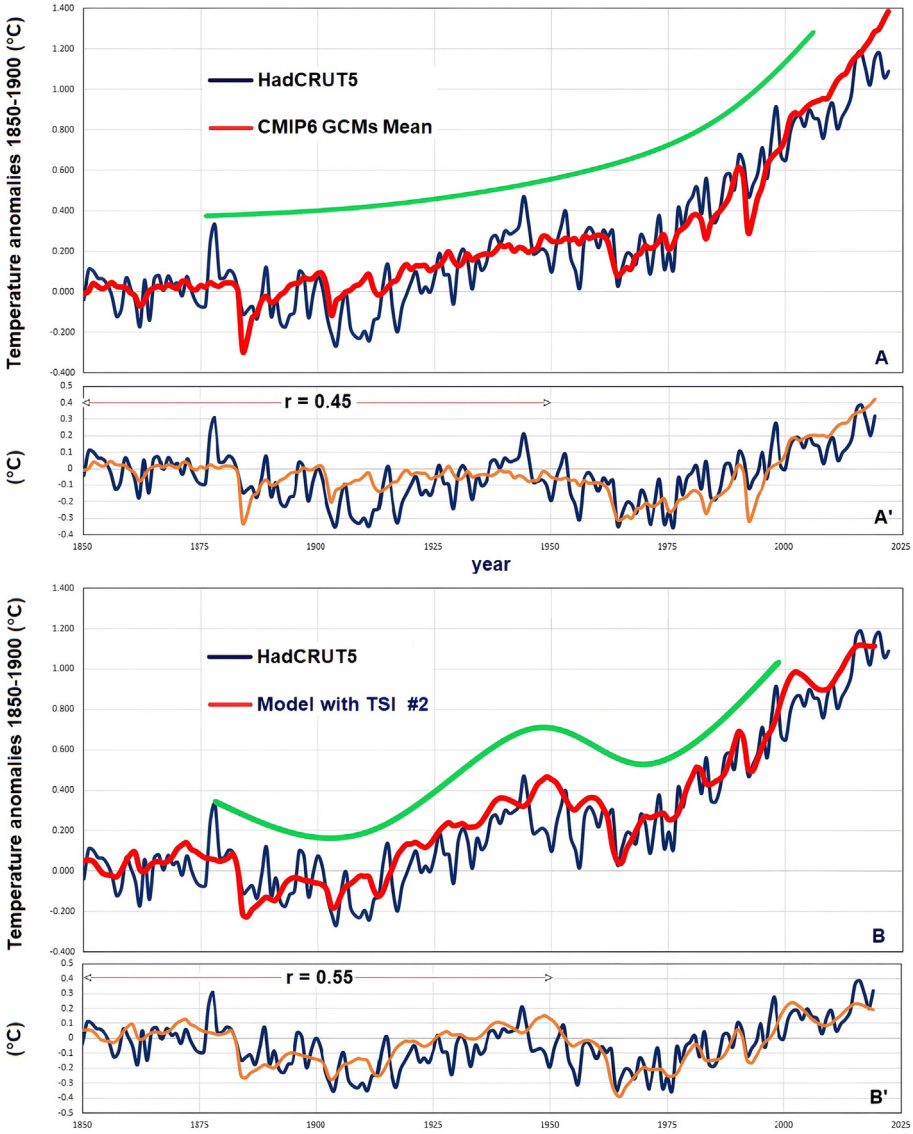

Fig. 8. (A) HadCRUT5 global surface temperature versus the CMIP6 GCM ensemble average; (A') the two records are detrended with the function f(t) = a $(x-1850)^2$. (B) HadCRUT5 global surface temperature versus the energy balance model (Eq. (16)) using the TSI proxy model #2; (B') the same as above. The green curves in Fig. 8A and B are sketches that highlight the different multi-decadal modulation of the red curves in Fig. 8A (monotonically increasing, like the anthropogenic forcing function) and in Fig. 8B (oscillating, like the temperature records). (For interpretation of the references to colour in this figure legend, the reader is referred to the web version of this article.)

2000 and 2014 before rising again since 2016 (due to the warming caused by the 11-year solar cycle maximum between 2012 and 2014 and a strong El-Niño event), which is a pattern that better correlates with the temperature record (blue curve).

Relative to the scenario discussed in Section 5.1, the ECS drops by 45% from a range equal to 1.4–2.8 °C with a mean of 2.1 °C, to a range equal to 0.8–1.8 °C with a mean of 1.2 °C using the HadCRUT4 and HadCRUT5 records. When the HadSST3 and HadSST4 records are utilized, the ECS decreases from 1.1 °C to 2.4 °C with a mean of 1.75 °C, to 0.6–1.6 °C with a mean of 1.0 °C.

Thus, ECS significantly decreases (by 40%–50%) by simply substituting the TSI record used in the CMIP6 GCMs with the proposed balanced TSI records and by using the latter as TSA proxies. The found new ECS range is significantly lower than the one reported by all CMIP6 GCMs, which ranges between 1.8 °C and 5.7 °C (Masson-Delmotte et al., 2021; Scafetta, 2023a). As a result, the CMIP6 GCMs are found to significantly overestimate the influence of anthropogenic forcing while failing to reveal the true impact of solar activity change on the climate. This is mostly because the Sun likely influences the climate through a variety of mechanisms, some of which are not directly related to TSI forcing alone.

The analysis also reveals that, especially after 1950, when the solar cycle is stronger, the peak-to-trough amplitude of the estimated temperature signature for the 11-year solar cycle is around 0.1 °C. Actually, many empirical studies (Douglass and Clader, 2002; Lean and Rind, 2008; Scafetta and West, 2008; Shaviv, 2008; Scafetta, 2009) would agree with this hindcast, which was also acknowledged by the IPCC (Solomon et al., 2007, p. 674). By contrast, when estimated as in Section 5.1, the same cycle has a peak-to-trough amplitude of 0.02–0.03 °C, which is what is generally hindcasted by the GCMs (Scafetta, 2013b) and by energy balance models that assume that the Sun only affects the climate by means of TSI forcing alone.

Lastly, the k_S/k_A ratio for the sea surface temperature records is 10%–20% greater than for the global surface temperature records. This finding implies that the global surface temperature on land may be warm-biased due to contamination from urban heat and other non-climatic warming mechanisms (Scafetta and Ouyang,

2019; Connolly et al., 2021; Scafetta, 2021a, 2023a). In fact, if non-climatic warm biases are not properly corrected, the climatic sensitivity to anthropogenic radiative forcing k_A would be overestimated relative to k_S.

6. Discussion

The Sun provides almost all the energy that warms the Earth's surface. Changes in its activity are expected to correlate with changes in the Earth's global surface temperature. Such a strong correlation has been observed by several authors (Eddy, 1976; Hoyt and Schatten, 1997; Svensmark and Friis-Christensen, 1997; Bond et al., 2001; Kerr, 2001; Douglass and Clader, 2002; Kirkby, 2007; Eichler et al., 2009; Scafetta, 2009; Steinhilber et al., 2012; Vahrenholt and Lüning, 2013; Svensmark et al., 2016; Miyahara et al., 2018; Easterbrook, 2019; Scafetta and Willson, 2019; Connolly et al., 2021; Schmutz, 2021; Svensmark, 2022). Nonetheless, there are many unanswered questions and ambiguities about how and to what extent changes in solar activity influence the climate. Usually, empirically-based studies find that solar activity changes have a considerable climatic impact, whilst studies based on present-day contemporary GCMs suggest that the Sun's role is modest. The dichotomy between empirical and GCM-based studies is very challenging and it is crucial for correctly interpreting climate change.

Several TSI proxy models have been developed (Hoyt and Schatten, 1993; Krivova et al., 2007, 2010; Steinhilber et al., 2012; Coddington et al., 2016, 2021; Egorova et al., 2018; Matthes et al., 2017; Wu et al., 2018; Penza et al., 2022, and others), and the TSI satellite composites since 1978 have been disputed (Willson and Mordvinov, 2003; Dewitte et al., 2004; Fröhlich, 2009; de Wit et al., 2017). Furthermore, changes in solar activity are not limited to total luminosity outputs, which define the TSI variable, but also include variations in spectrum frequencies (e.g., UV varies differently than visible light), magnetic activity variations, solar wind variations, and modulation of fluxes of galactic cosmic rays and interplanetary dust. Solar activity changes alter the space weather surrounding the Earth (Moldwin, 2022) and can influence the climate system throughout a variety of physical mechanisms such as direct TSI forcing, direct cloud system modulation, stratospheric ozone layer modulation, global atmospheric and oceanic circulation modulation, biosphere modulation, and so on.

The IPCC (Solomon et al., 2007; Stocker et al., 2014; Masson-Delmotte et al., 2021) conclusion that the Sun's role in climate change has been negligible since the pre-industrial period (1850–1900) derives from the fact that this organization only consider the solar climatic signature produced by the present-day GCMs. These models, however, are computer programs that can only employ equations describing physical mechanisms that are already well known. Anything unknown or ambiguous cannot be included in the GCM software. If the climatic influence of neglected physical processes is significant, the reductionist approach employed in the GCMs for assessing climate change attributions may be severely inappropriate for the task.

Furthermore, the CMIP6 GCMs used the TSI solar forcing function proposed by Matthes et al. (2017), which exhibits a very modest multidecadal and secular variability, and, consequently, concluded that anthropogenic emissions account for nearly all of the observed global warming since the pre-industrial period (1850–1900). Thus, according to the IPCC, solar activity variations have been irrelevant for reproducing the observed global surface temperature changes of the last 150 years (Masson-Delmotte et al., 2021).

However, it cannot be ignored that several empirically-based studies have found a robust association between variations in solar activity and climate records throughout the Holocene at multiple time scales (Eddy, 1976; Hoyt and Schatten, 1997; Svensmark and Friis-Christensen, 1997; Bond et al., 2001; Kerr, 2001; Douglass and Clader, 2002; Kirkby, 2007; Eichler et al., 2009; Scafetta, 2009; Steinhilber et al., 2012; Vahrenholt and Lüning, 2013; Svensmark et al., 2016; Scafetta and Willson, 2019; Connolly et al., 2021; Schmutz, 2021; Svensmark, 2022; Easterbrook, 2019; and many others).

Indeed, the TSI model used by the CMIP6 GCMs is not the only TSI record available in scientific literature. There are additional TSI proxy reconstructions that show a distinct modulation and a significant multidecadal and secular variability (Hoyt and Schatten, 1993; Scafetta and Willson, 2014; Egorova et al., 2018; Scafetta et al., 2019). Studies on Sun-like stars (Judge et al., 2020), the ACRIM TSI satellite composite (Willson and Mordvinov, 2003; Scafetta et al., 2019), which is based on the actual published TSI satellite observations from 1978 to 2013, and other types of solar modeling based on planetary tidal forcing appear to support them (Scafetta, 2012a, 2014; Scafetta and Bianchini, 2022).

I proposed to replace Matthes et al. (2017)'s TSI proxy model with three new TSI proxy records based on different pairings of the most popular low and high secular-variability TSI proxy models currently available: see Fig. 3. These datasets were interpreted as TSA functions and climate forcings in a simple energy balance model that was calibrated using a novel differential multi-linear regression analysis methodology, which could in first approximation assess the climatic influence of TSA changes and their importance relative to TSI forcing alone. The key findings were the following.

(i) If the TSI forcing used by the CMIP6 GCMs is adopted and the climate system is assumed to be solely sensitive to radiative forcings, the proposed modeling confirms the IPCC's conclusion (Masson-Delmotte et al., 2021) that anthropogenic emissions account for substantially all of the observed global warming since the pre-industrial period (1850–1900) and that changes in solar activity are practically irrelevant. In this scenario, the ECS was estimated to be 2.0 ± 0.7 °C (by averaging the results obtained with the four analyzed temperature records), which roughly corresponds to what has been discovered by some recent studies (Lewis and Curry, 2018; Scafetta, 2021c, 2022, 2023a; Lewis, 2023). This range is roughly covered by the CMIP6 GCMs with ECS between 1.8 and 3.0 °C. Under identical physical conditions, if the TSI forcing is replaced with the three balanced TSI functions, the Sun could have contributed no more than 10% of the observed warming. As a result, in either case, TSI forcing does not appear to have a significant influence on climate change. To do so, TSI secular variations should be demonstrated to be substantially larger than what is currently shown even by the high secular-variability TSI proxy models, as recently suggested by Schmutz (2021).

(ii) If the TSI forcing adopted by the CMIP6 GCMs is employed, but it is supposed to represent a proxy for TSA changes that might influence the climate in a variety of (known and unknown) ways, the proposed modeling implies that the TSA impact on the climate could be 4.3 ± 2.5 times bigger than the TSI effect alone. This finding implies that most of the solar effect on climate could be caused by mechanisms other than TSI forcing alone. Possible candidates are corpuscular forcings modulated by solar magnetic activity (cosmic rays, solar wind, etc.) or some other kind of corpuscular forcing (e.g. interplanetary dust fluxes) modulated by planetary resonances (which may also synchronize solar activity changes) that could directly influence the cloud system (Svensmark and Friis-Christensen, 1997; Shaviv, 2002; Svensmark et al., 2016; Scafetta et al., 2020; Svensmark, 2022). In this scenario, the ECS is found to be only slightly smaller than in the previous case, on average

1.8 ± 0.6 °C, because the adopted solar record (Matthes et al., 2017) has a very small multi-decadal and secular variability, which is also poorly correlated with the climatic records.

(iii) If the solar record by Matthes et al. (2017) is replaced with the three proposed balanced TSI forcing functions (see Fig. 4), and these functions are assumed to be proxies for TSA changes that can influence the climate in various (known and unknown) ways, the proposed modeling suggests that the solar total impact on the climate could be 4–7 times greater than its TSI effect alone. Solar activity changes could have a considerable climatic impact that could be almost comparable with the anthropogenic component (compare the yellow and blue curves in Figs. 6 and 7). Moreover, the modeled temperature hindcasts are better correlated with global and sea surface temperature records. Figs. 6 and 7 also demonstrate that the solar models #1 and #2 (Supplementary Data Tables S2 and S3) outperform the model #3 (Supplementary Data Table S4), which gives more weight to the low secular-variability TSI proxy models. In these scenarios, the ECS considerably decreases from an average of 2.0 ± 0.7 °C (see case 1), to an average of 1.1 ± 0.3 °C: a drop of 45%. This ECS range is much lower than the ECS values predicted by the CMIP6 GCMs (which ranges from 1.8 °C to 5.7 °C), but it is nevertheless consistent with a number of independent studies (Scafetta, 2009, 2010, 2013a; Lindzen and Choi, 2011; Harde, 2014; Loehle, 2014; Monckton et al., 2015; Bates, 2016; McKitrick and Christy, 2020; Stefani, 2021). The result largely supports the hypothesis advanced by Scafetta (2012b, 2013a), if the climate system is characterized by a (presumably solar-generated) quasi 60-year natural oscillation (likely generated by solar/astronomical forcings) that the GCMs cannot reproduce, the actual ECS must be about half of that predicted by the GCMs that better hindcast the global warming from 1970 to 2020. Since Scafetta (2022, 2023a,b) showed that the most accurate CMIP6 GCM subset appears to be the one made with GCMs with ECS between 1.8 °C and 3.0 °C, halving this range yields 0.9–1.5 °C, which approximately matches the aforementioned finding.

The climate's real sensitivity to TSA changes, k_S, is found to be 4–7 times greater than the sensitivity to radiative forcing alone, denoted by $k_{AV} = k_A = k_V$. Moreover, the significant positive correlation between solar proxy and climatic records observed during the Holocene (Hoyt and Schatten, 1993, 1997; Cliver et al., 1998; Kerr, 2001; Neff et al., 2001; Fleitmann et al., 2003; Hu et al., 2003; Shaviv and Veizer, 2003; Scafetta et al., 2004; Scafetta and West, 2006; Kirkby, 2007; Eichler et al., 2009; Scafetta, 2009, 2011; Mufti and Shah, 2011; Steinhilber et al., 2012; Scafetta, 2013a; Soon and Legates, 2013; Vahrenholt and Lüning, 2013; Connolly et al., 2021; Schmutz, 2021; Bond et al., 2001; Easterbrook, 2019; Taricco et al., 2022, and many others) can be explained only if the Sun's role in climate change is significant. Hence, either TSI variations are substantially bigger than how they are now reconstructed, as Schmutz (2021) suggested, or there are key solar-climate mechanisms complementary to TSI forcing that are still poorly understood and, therefore, ignored in the present-day GCMs.

These results approximately agree and explain the results of Soon et al. (2000) who found that the climate appears to be hypersensitive to solar forcing, with those of Shaviv (2008) who analyzed the signature of the 11-year solar cycle in the ocean and concluded that it could be about 5–7 times larger than just that associated with the TSI variations alone, and of Ziskin and Shaviv (2012) who found that the total solar contribution to the 20th century global warming appears to be much greater than could be expected from variation in the total solar irradiance alone.

Table 1 also reports the estimated TCR values in all cases, which were calculated with Eq. (7). TCR is usually found to be slightly smaller than the correspondent ECS values (1.1 ± 0.3 °C) because the evaluated characteristic time responses τ are just a few years: τ is found to be on average 6.7 ± 1.7 years by using the GCM TSI record, and 3.6 ± 0.6 years by using the new proposed TSI records as TSA proxies.

The proposed analysis suggests that if the actual TSI secular variations are comparable with the three suggested balanced TSI functions and TSA is sufficiently proportional to them, then the actual TSA effect on the climate could be about 5 times greater than the TSI effect alone.

7. Conclusion

The IPCC (Masson-Delmotte et al., 2021) assertion that the warming observed since the pre-industrial period (1850–1900) is almost entirely due to anthropogenic emissions is based solely on the results of certain GCMs that assume that variations in solar activity can only have an impact on the climate through total solar irradiance (TSI) and solar spectral irradiance (SSI) radiative forcings. Furthermore, these GCMs use a radiative forcing function derived from the low secular-variability TSI proxy models proposed in the scientific literature (Matthes et al., 2017). This choice minimizes the solar component of climate change while maximizing the anthropogenic one.

Under the aforementioned conditions, the actual ECS should range from 1.4 °C to 2.8 °C with a mean of 2.1 °C, implying that only the CMIP6 GCMs compatible with such a low-ECS range could be safely used for public policies that aim to mitigate future climate change hazards, as Scafetta (2022, 2023a, 2023b) already indicated. This ECS range is also compatible with the recent results by Lewis (2023), who utilized the same forcings.

However, the scientific literature also provides TSI proxy models with substantially larger multi-decadal and secular variability. These TSI proxy models should not be ignored in climate change research. Integrating the most popular TSI records made it possible to take into consideration all common proxies used to recreate solar activity changes. Following that, three unique TSI multi-proxy models were proposed. They show a greater TSI variability as well as a unique temporal modulation that matches more closely the temperature records.

To assess their climatic relevance, I applied a differential multilinear regression model that approximates the thermodynamic response of the climate system while also accounting for the climatic effects of both anthropogenic and volcanic activities. The adopted modeling also allows for a more complex response of the climate to changes in solar activity than could be achievable with just radiative forcing. This property is crucial because the Sun likely influence Earth's climate by means of both radiative and non-radiative forcings, with the latter mostly linked to its magnetic activity that can directly modulate cosmic ray fluxes and generate space weather perturbations.

The obtained climate simulations from 1850 to 2020 are found to be better correlated with the available global and sea surface temperature records, especially if the TSI records #1 and #2 are used. In particular, the TSI #2 excludes the low secular-variability TSI proxy models by Matthes et al. (2017) and appears to be the best performing solar model. The anthropogenic impact was found to be substantially lower, and the solar effect on climate was found to be much more significant than what the IPCC acknowledged (Solomon et al., 2007; Stocker et al., 2014; Masson-Delmotte et al., 2021). The ECS was determined to be 0.8–1.8 °C with a mean of roughly 1.2 °C using the global surface temperature records, and 0.6–1.6 °C with a mean of roughly 1.0 °C using the sea surface temperature records.

The found ECS range is significantly lower than either what predicted by the CMIP6 GCMs (1.8–5.7 °C) and the likely ECS range claimed by the IPCC AR6 (2.5–4.0 °C). However, low ECS estimates

are consistent with several independent empirical investigations that have highlighted an important role of the Sun and of the natural variability in determining what has caused climate changes since 1850. In particular, the found low range for the likely ECS is compatible with the ECS ranges recently estimated by McKitrick and Christy (2020), who found a pervasive warming bias in all CMIP6 GCMs when their hindcasts are compared against the troposphere temperature records, and by Stefani (2021). The latter author used a regression algorithm finalized to assess the solar and anthropogenic influences on climate based on the geomagnetic aa-index record, which approximately exhibits a long-term variability like that of the three TSA records herein proposed. This agreement might also provide a strong posterior argument for the plausibility of the proposed TSA models.

ECS values near to 1.0 °C would imply that the positive and negative feedbacks to radiative forcing are roughly balanced. In fact, doubling the concentration of CO_2 in the atmosphere from 280 ppm to 560 ppm might theoretically generate, by alone, a warming of roughly 1.0 °C (Rahmstorf, 2008). Thus, another key result of this study is that, on average, the total climatic feedback to CO_2 changes could only be slightly positive. Moreover, it should also be taken into account that part of the warming shown by the official surface temperature data may be fictitious because it could result from urban heat islands and other non-climatic biases (Connolly et al., 2021; Scafetta, 2021a, 2023b). Thus, perhaps, the ECS values evaluated with the SST records (around 1 °C) might be more realistic.

The CMIP6 GCMs appear to greatly underestimate the Sun's role in climate change because of two major limitations: (i) erroneous solar forcings have likely been integrated into the models; and (ii) TSI alone appears to likely be not the most important solar forcing. Additional solar-magnetism related forcings and associated mechanisms are not included in the GCMs because they are currently poorly understood, despite the fact that there are several empirical indications that they might sufficiently modulate the cloud cover system (by 5% or less) to explain a significant component of the observed climatic changes (Svensmark and Friis-Christensen, 1997; Shaviv, 2002; Svensmark et al., 2016; Easterbrook, 2019; Svensmark, 2022). In fact, Table 1 shows that the actual climate sensitivity to TSA variations, which is expressed by k_S, can be 4–7 times greater than the climate sensitivity to radiative forcing alone, which was denoted by k_A.

Thus, at least about 80% of the solar influence on the climate could be generated by processes other than direct TSI forcing. If this result is correct, several solar-climate mechanisms must be thoroughly investigated and fully understood before reliable GCMs can be developed.

CRediT authorship contribution statement

Nicola Scafetta: Conceptualization, Formal analysis, Methodology, Writing – original draft, Writing – review & editing.

Declaration of Competing Interest

The author declares that he has no known competing financial interests or personal relationships that could have appeared to influence the work reported in this paper.

Acknowledgement

This research received no external funding.

Data availability

The forcing data used in the paper can be downloaded from (accessed on 05/05/2023): Effective Radiative Forcings:
https://zenodo.org/record/5705391/files/table_A3.3_historical_ERF_1750-2019_best_estimate.csv,
https://github.com/chrisroadmap/ar6/blob/main/data_output/AR6_ERF_1750-2019.csv;
RegressItPC: https://regressit.com/regressitpc.html.

Appendix A. Supplementary data

Supplementary data 1 and 2 to this article can be found online at https://doi.org/10.1016/j.gsf.2023.101650.

References

Ball, W.T., Unruh, Y.C., Krivova, N.A., Solanki, S., Wenzler, T., Mortlock, D.J., Jaffe, A. H., 2012. Reconstruction of total solar irradiance 1974–2009. Astron. Astrophys. 541, A27.
Bates, J.R., 2016. Estimating climate sensitivity using two-zone energy balance models. Earth Space Sci. 3 (5), 207–225.
Bond, G., Kromer, B., Beer, J., Muscheler, R., Evans, M.N., Showers, W., Hoffmann, S., Lotti-Bond, R., Hajdas, I., Bonani, G., 2001. Persistent solar influence on North Atlantic climate during the holocene. Science 294 (5549), 2130–2136.
Bragato, P.L., 2015. Italian seismicity and vesuvius' eruptions synchronize on a quasi 60 year oscillation. Earth Space Sci. 2 (5), 134–143.
Cliver, E.W., Boriakoff, V., Feynman, J., 1998. Solar variability and climate change: Geomagnetic aa index and global surface temperature. Geophys. Res. Lett. 25 (7), 1035–1038.
Coddington, O., Lean, J.L., Pilewskie, P., Snow, M., Lindholm, D., 2016. A solar irradiance climate data record. Bull. Am. Meteorol. Soc. 97 (7), 1265–1282.
Coddington, O.M., Richard, E.C., Harber, D., Pilewskie, P., Woods, T.N., Chance, K., Liu, X., Sun, K., 2021. The TSIS-1 hybrid solar reference spectrum. Geophys. Res. Lett. 48 (12). e2020GL091709.
Connolly, R., Soon, W., Connolly, M., Baliunas, S., Berglund, J., Butler, C.J., Cionco, R. G., Elias, A.G., Fedorov, V.M., Harde, H., Henry, G.W., Hoyt, D.V., Humlum, O., Legates, D.R., Lüning, S., Scafetta, N., Solheim, J.-E., Szarka, L., van Loon, H., Herrera, V.M.V., Willson, R.C., Yan, H., Zhang, W., 2021. How much has the sun influenced northern hemisphere temperature trends? An ongoing debate. Res. Astron. Astrophys. 21 (6), 131.
de Wit, T.D., Kopp, G., Fröhlich, C., Schöll, M., 2017. Methodology to create a new total solar irradiance record: Making a composite out of multiple data records. Geophys. Res. Lett. 44 (3), 1196–1203.
Dewitte, S., Crommelynck, D., Mekaoui, S., Joukoff, A., 2004. Measurement and uncertainty of the long-term total solar irradiance trend. Sol. Phys. 224 (1–2), 209–216.
Douglass, D.H., Clader, B.D., 2002. Climate sensitivity of the earth to solar irradiance. Geophys. Res. Lett. 29 (16). 33.1–4.
Easterbrook, D.J., 2019. Solar Magnetic Cause of Climate Changes and Origin of the Ice Ages. Independently Published.
Eddy, J.A., 1976. The maunder minimum. Science 192 (4245), 1189–1202.
Egorova, T., Schmutz, W., Rozanov, E., Shapiro, A.I., Usoskin, I., Beer, J., Tagirov, R.V., Peter, T., 2018. Revised historical solar irradiance forcing. Astron. Astrophys. 615, A85.
Eichler, A., Olivier, S., Henderson, K., Laube, A., Beer, J., Papina, T., Gäggeler, H.W., Schwikowski, M., 2009. Temperature response in the Altai region lags solar forcing. Geophys. Res. Lett. 36 (1), L01808.
Eyring, V., Bony, S., Meehl, G.A., Senior, C.A., Stevens, B., Stouffer, R.J., Taylor, K.E., 2016. Overview of the coupled model intercomparison project phase 6 (CMIP6) experimental design and organization. Geosci. Model Dev. 9 (5), 1937–1958.
Fleitmann, D., Burns, S.J., Mudelsee, M., Neff, U., Kramers, J., Mangini, A., Matter, A., 2003. Holocene forcing of the indian monsoon recorded in a stalagmite from southern Oman. Science 300 (5626), 1737–1739.
Fröhlich, C., 2009. Evidence of a long-term trend in total solar irradiance. Astron. Astrophys. 501 (3), L27–L30.
Fröhlich, C., 2012. Total solar irradiance observations. Surv. Geophys. 33 (3–4), 453–473.
Fröhlich, C., Lean, J.L., 1998. The sun's total irradiance: Cycles, trends and related climate change uncertainties since 1976. Geophys. Res. Lett. 25 (23), 4377–4380.
Gleisner, H., Thejll, P., 2003. Patterns of tropospheric response to solar variability. Geophys. Res. Lett. 30 (13), 1711.
Harde, H., 2014. Advanced two-layer climate model for the assessment of global warming by CO2. Open J. Atmos. Clim. Change 2014 (3), 1–51.
Herdiwijaya, D., Arif, J., Nurzaman, M.Z., 2014. On the relation between solar and global volcanic activities. In: Proceedings of the 2014 International Conference on Physics. Atlantis Press, pp. 105–108.
Hofer, S., Tedstone, A.J., Fettweis, X., Bamber, J.L., 2017. Decreasing cloud cover drives the recent mass loss on the Greenland ice sheet. Sci. Adv. 3 (6), e170058.

Hoyt, D.V., Schatten, K.H., 1993. A discussion of plausible solar irradiance variations, 1700–1992. J. Geophys. Res. Space Phys. 98 (A11), 18895–18906.
Hoyt, D.V., Schatten, K.H., 1997. The Role of the Sun in Climate Change. Oxford University Press.
Hu, F.S., Kaufman, D., Yoneji, S., Nelson, D., Shemesh, A., Huang, Y., Tian, J., Bond, G., Clegg, B., Brown, T., 2003. Cyclic variation and solar forcing of holocene climate in the Alaskan Subarctic. Science 301 (5641), 1890–1893.
Judge, P.G., Egeland, R., Henry, G.W., 2020. Sun-like stars shed light on solar climate forcing. Astrophys. J. 891 (1), 96.
Kennedy, J.J., Rayner, N.A., Smith, R.O., Parker, D.E., Saunby, M., 2011a. Reassessing biases and other uncertainties in sea surface temperature observations measured in situ since 1850: 1. Measurement and sampling uncertainties. J. Geophys. Res. 116 (D14) D14103.
Kennedy, J.J., Rayner, N.A., Smith, R.O., Parker, D.E., Saunby, M., 2011b. Reassessing biases and other uncertainties in sea surface temperature observations measured in situ since 1850: 2. Biases and homogenization. J. Geophys. Res. 116 (D14) D14104.
Kennedy, J.J., Rayner, N.A., Atkinson, C.P., Killick, R.E., 2019. An ensemble data set of sea surface temperature change from 1850: The met office Hadley centre HadSST.4.0.0.0 data set. J. Geophys. Res. Atmos. 124 (14), 7719–7763.
Kerr, R.A., 2001. A variable sun paces millennial climate. Science 294 (5546), 1431–1433.
Kirkby, J., 2007. Cosmic rays and climate. Surv. Geophys. 28 (5–6), 333–375.
Kopp, G., Lean, J.L., 2011. A new, lower value of total solar irradiance: Evidence and climate significance. Geophys. Res. Lett. 38 (1) L01706.
Krivova, N.A., Balmaceda, L., Solanki, S.K., 2007. Reconstruction of solar total irradiance since 1700 from the surface magnetic flux. Astron. Astrophys. 467 (1), 335–346.
Krivova, N.A., Vieira, L.E.A., Solanki, S.K., 2010. Reconstruction of solar spectral irradiance since the Maunder minimum. J. Geophys. Res. Space Phys. 115 (A12) A12112.
Lean, J.L., Beer, J., Bradley, R., 1995. Reconstruction of solar irradiance since 1610: Implications for climate change. Geophys. Res. Lett. 22 (23), 3195–3198.
Lean, J.L., Rind, D.H., 2008. How natural and anthropogenic influences alter global and regional surface temperatures: 1889 to 2006. Geophys. Res. Lett. 35 (18) L18701.
Lewis, N., 2023. Objectively combining climate sensitivity evidence. Clim. Dyn. 60, 3139–3165.
Lewis, N., Curry, J., 2018. The impact of recent forcing and ocean heat uptake data on estimates of climate sensitivity. J. Clim. 31 (15), 6051–6071.
Lindsey, R., 2003. Under a Variable Sun. NASA's Earth Observatory. https://earthobservatory.nasa.gov/features/VariableSun/variable4.php.
Lindzen, R.S., Choi, Y.-S., 2011. On the observational determination of climate sensitivity and its implications. Asia-Pac. J. Atmos. Sci. 47 (4), 377–390.
Lockwood, M., Ball, W.T., 2020. Placing limits on long-term variations in quiet-sun irradiance and their contribution to total solar irradiance and solar radiative forcing of climate. Proc. Royal Soc. A: Math. Phys. Eng. Sci. 476 (2238) 20200077.
Loehle, C., 2014. A minimal model for estimating climate sensitivity. Ecol. Model. 276, 80–84.
Loehle, C., Scafetta, N., 2011. Climate change attribution using empirical decomposition of climatic data. Open Atmos. Sci. J. 5 (1), 74–86.
Marshall, L.R., Smith, C.J., Forster, P.M., Aubry, T.J., Andrews, T., Schmidt, A., 2020. Large variations in volcanic aerosol forcing efficiency due to eruption source parameters and rapid adjustments. Geophys. Res. Lett. 47 (19). e2020GL090241.
Masson-Delmotte, V. et al., 2021. Climate Change 2021 The Physical Science Basis: Assessment Working Group I Contribution to the IPCC Sixth Assessment Report. Cambridge University Press.
Matthes, K., Funke, B., Andersson, M.E., Barnard, L., Beer, J., Charbonneau, P., Clilverd, M.A., de Wit, T.D., Haberreiter, M., Hendry, A., Jackman, C.H., Kretzschmar, M., Kruschke, T., Kunze, M., Langematz, U., Marsh, D.R., Maycock, A.C., Misios, S., Rodger, C.J., Scaife, A.A., Seppälä, A., Shangguan, M., Sinnhuber, M., Tourpali, K., Usoskin, I., van de Kamp, M., Verronen, P.T., Versick, S., 2017. Solar forcing for CMIP6 (v3.2). Geosci. Model Dev. 10 (6), 2247–2302.
Mazzarella, A., Palumbo, A., 1989. Does the solar cycle modulate seismic and volcanic activity? J. Volcanol. Geoth. Res. 39 (1), 89–93.
McKitrick, R., Christy, J., 2020. Pervasive warming bias in CMIP6 tropospheric layers. Earth and Space. Science 7 (9). e2020EA001281.
Miyahara, H., Kataoka, R., Mikami, T., Zaiki, M., Hirano, J., Yoshimura, M., Aono, Y., Iwahashi, K., 2018. Solar rotational cycle in lightning activity in japan during the 18–19th centuries. Ann. Geophys. 36 (2), 633–640.
Moberg, A., Sonechkin, D.M., Holmgren, K., Datsenko, N.M., Karlén, W., 2005. Highly variable northern hemisphere temperatures reconstructed from low- and high-resolution proxy data. Nature 433 (2), 613–617.
Moldwin, M., 2022. Introduction to Space Weather. Cambridge University Press.
Monckton, C., Soon, W.-W.-H., Legates, D.R., Briggs, W.M., 2015. Why models run hot: results from an irreducibly simple climate model. Sci. Bull. 60 (1), 122–135.
Morice, C.P., Kennedy, J.J., Rayner, N.A., Jones, P.D., 2012. Quantifying uncertainties in global and regional temperature change using an ensemble of observational estimates: The HadCRUT4 data set. J. Geophys. Res. Atmos. 117 (D8) D08101.
Morice, C.P., Kennedy, J.J., Rayner, N.A., Winn, J.P., Hogan, E., Killick, R.E., Dunn, R.J. H., Osborn, T.J., Jones, P.D., Simpson, I.R., 2021. An updated assessment of near-surface temperature change from 1850: The HadCRUT5 data set. J. Geophys. Res. Atmos. 126 (3). e2019JD032361.
Mufti, S., Shah, G., 2011. Solar-geomagnetic activity influence on earth's climate. J. Atmos. Sol. Terr. Phys. 73 (13), 1607–1615.
Neff, U., Burns, S.J., Mangini, A., Mudelsee, M., Fleitmann, D., Matter, A., 2001. Strong coherence between solar variability and the monsoon in Oman between 9 and 6 kyr ago. Nature 411 (6835), 290–293.
Penza, V., Berrilli, F., Bertello, L., Cantoresi, M., Criscuoli, S., Giobbi, P., 2022. Total solar irradiance during the last five centuries. Astrophys. J. 937 (2), 84.
Pfeifroth, U., Sanchez-Lorenzo, A., Manara, V., Trentmann, J., Hollmann, R., 2018. Trends and variability of surface solar radiation in europe based on surface- and satellite-based data records. J. Geophys. Res. Atmos. 123 (3), 1735–1754.
Pokrovsky, O.M., 2019. Cloud changes in the period of global warming: The results of the international satellite project. Izv. Atmos. Ocean. Phys. 55 (9), 1189–1197.
Rahmstorf, S., 2008. Anthropogenic Climate Change: Revisiting the Facts. Brookings Institution Press. Ch. 3, http://www.jstor.org/stable/10.7864/j.ctt127xgs.7.
Richard, E., Harber, D., Coddington, O., Drake, G., Rutkowski, J., Triplett, M., Pilewskie, P., Woods, T., 2020. SI-traceable spectral irradiance radiometric characterization and absolute calibration of the TSIS-1 spectral irradiance monitor (SIM). Remote Sens. (Basel) 12 (11), 1818.
Richardson, M.T., Benestad, R.E., 2022. Erroneous use of statistics behind claims of a major solar role in recent warming. Res. Astron. Astrophys. 22 (12) 125008.
Scafetta, N., 2008. Comment on "heat capacity, time constant, and sensitivity of earth's climate system" by s. e. Schwartz. J. Geophys. Res. 113 (D15) D15104.
Scafetta, N., 2009. Empirical analysis of the solar contribution to global mean air surface temperature change. J. Atmos. Sol. Terr. Phys. 71 (17–18), 1916–1923.
Scafetta, N., 2010. Empirical evidence for a celestial origin of the climate oscillations and its implications. J. Atmos. Sol. Terr. Phys. 72 (13), 951–970.
Scafetta, N., 2011. Total solar irradiance satellite composites and their phenomenological effect on climate. In: Evidence-Based Climate Science. Elsevier, pp. 289–316.
Scafetta, N., 2012a. Multi-scale harmonic model for solar and climate cyclical variation throughout the holocene based on Jupiter-Saturn tidal frequencies plus the 11-year solar dynamo cycle. J. Atmos. Sol. Terr. Phys. 80, 296–311.
Scafetta, N., 2012b. Testing an astronomically based decadal-scale empirical harmonic climate model versus the IPCC (2007) general circulation climate models. J. Atmos. Sol. Terr. Phys. 80, 124–137.
Scafetta, N., 2013a. Discussion on climate oscillations: CMIP5 general circulation models versus a semi-empirical harmonic model based on astronomical cycles. Earth Sci. Rev. 126, 321–357.
Scafetta, N., 2013b. Discussion on common errors in analyzing sea level accelerations, solar trends and global warming. Pattern Recogn. Phys. 1 (1), 37–57.
Scafetta, N., 2013c. Multi-scale dynamical analysis (MSDA) of sea level records versus PDO, AMO, and NAO indexes. Clim. Dyn. 43 (1–2), 175–192.
Scafetta, N., 2014. Discussion on the spectral coherence between planetary, solar and climate oscillations: a reply to some critiques. Astrophys. Space Sci. 354 (2), 275–299.
Scafetta, N., 2021a. Detection of non-climatic biases in land surface temperature records by comparing climatic data and their model simulations. Clim. Dyn. 56 (9–10), 2959–2982.
Scafetta, N., 2021b. Reconstruction of the interannual to millennial scale patterns of the global surface temperature. Atmosphere 12 (2), 147.
Scafetta, N., 2021c. Testing the CMIP6 GCM simulations versus surface temperature records from 1980–1990 to 2011–2021: High ECS is not supported. Climate 9 (11), 161.
Scafetta, N., 2022. Advanced testing of low, medium, and high ECS CMIP6 GCM simulations versus ERA5-t2m. Geophys. Res. Lett. 49 (6). e2022GL097716.
Scafetta, N., 2023a. CMIP6 GCM ensemble members versus global surface temperatures. Clim. Dyn. 60, 3091–3120.
Scafetta, N., 2023b. CMIP6 GCM validation based on ECS and TCR ranking for 21st century temperature projections and risk assessment. Atmosphere 14 (2), 345.
Scafetta, N., Bianchini, A., 2022. The planetary theory of solar activity variability: A review. Front. Astron. Space Sci. 9 937930.
Scafetta, N., West, B.J., 2008. Variations on sun's role in climate change. Phys. Today 61 (10), 14–16.
Scafetta, N., Willson, R.C., 2009. ACRIM-GAP and TSI trend issue resolved using a surface magnetic flux TSI proxy model. Geophys. Res. Lett. 36 (5) L05701.
Scafetta, N., Willson, R.C., 2014. ACRIM total solar irradiance satellite composite validation versus TSI proxy models. Astrophys. Space Sci. 350 (2), 421–442.
Scafetta, N., Willson, R.C., 2019. Comparison of decadal trends among total solar irradiance composites of satellite observations. Adv. Astron. 2019, 1–14.
Scafetta, N., Grigolini, P., Imholt, T., Roberts, J., West, B.J., 2004. Solar turbulence in earth's global and regional temperature anomalies. Phys. Rev. E 69 (2) 026303.
Scafetta, N., Mazzarella, A., 2015. Spectral coherence between climate oscillations and the M $\geq$ 7 earthquake historical worldwide record. Nat. Hazards 76 (3), 1807–1829.
Scafetta, N., Ouyang, S., 2019. Detection of UHI bias in china climate network using tmin and tmax surface temperature divergence. Glob. Planet. Change 181 102989.
Scafetta, N., West, B.J., 2005. Estimated solar contribution to the global surface warming using the ACRIM TSI satellite composite. Geophys. Res. Lett. 32 (18) L18713.
Scafetta, N., West, B.J., 2006. Phenomenological solar signature in 400 years of reconstructed northern hemisphere temperature record. Geophys. Res. Lett. 33 (17) L17718.

Scafetta, N., Willson, R., Lee, J., Wu, D., 2019. Modeling quiet solar luminosity variability from TSI satellite measurements and proxy models during 1980–2018. Remote Sens. (Basel) 11 (21), 2569.
Scafetta, N., Milani, F., Bianchini, A., 2020. A 60-year cycle in the meteorite fall frequency suggests a possible interplanetary dust forcing of the earth's climate driven by planetary oscillations. Geophys. Res. Lett. 47 (18). e2020GL089954.
Schmutz, W.K., 2021. Changes in the total solar irradiance and climatic effects. J. Space Weather Space Clim. 11, 40.
Shapiro, A.I., Schmutz, W., Rozanov, E., Schoell, M., Haberreiter, M., Shapiro, A.V., Nyeki, S., 2011. A new approach to the long-term reconstruction of the solar irradiance leads to large historical solar forcing. Astron. Astrophys. 529, A67.
Shaviv, N.J., 2002. Cosmic ray diffusion from the galactic spiral arms, iron meteorites, and a possible climatic connection. Phys. Rev. Lett. 89 (5) 051102.
Shaviv, N.J., 2008. Using the oceans as a calorimeter to quantify the solar radiative forcing. J. Geophys. Res. Space Phys. 113 (A11). A11101.
Shaviv, N.J., Veizer, J., 2003. Celestial driver of phanerozoic climate? GSA Today 13 (7), 4–10.
Solomon, S. et al., 2007. Climate Change 2007 The Physical Science Basis: Assessment Working Group I Contribution to the IPCC Fourth Assessment Report. Cambridge University Press.
Soon, W., Legates, D.R., 2013. Solar irradiance modulation of equator-to-pole (arctic) temperature gradients: Empirical evidence for climate variation on multi-decadal timescales. J. Atmos. Sol. Terr. Phys. 93, 45–56.
Soon, W., Posmentier, E., Baliunas, S., 2000. Climate hypersensitivity to solar forcing? Ann. Geophys. 18 (5), 583–588.
Stefani, F., 2021. Solar and anthropogenic influences on climate: Regression analysis and tentative predictions. Climate 9 (11), 163.
Steinhilber, F., Abreu, J. A., Beer, J., Brunner, I., Christl, M., Fischer, H., Heikkilä, U., Kubik, P. W., Mann, M., McCracken, K. G., Miller, H., Miyahara, H., Oerter, H., Wilhelms, F., 2012. 9,400 years of cosmic radiation and solar activity from ice cores and tree rings. Proc. Natl. Acad. Sci. U.S.A. 109 (16), 5967–5971.
Stocker, T.F. et al., 2014. Climate Change 2013 The Physical Science Basis: Assessment Working Group I Contribution to the IPCC Fifth Assessment Report. Cambridge University Press.
Stothers, R.B., 1989. Volcanic eruptions and solar activity. J. Geophys. Res. 94 (B12), 17371.
Svensmark, H., 2022. Supernova rates and burial of organic matter. Geophys. Res. Lett. 49 (1). e2021GL096376.
Svensmark, J., Enghoff, M.B., Shaviv, N.J., Svensmark, H., 2016. The response of clouds and aerosols to cosmic ray decreases. J. Geophys. Res. Space Phys. 121 (9), 8152–8181.
Svensmark, H., Friis-Christensen, E., 1997. Variation of cosmic ray flux and global cloud coverage – a missing link in solar-climate relationships. J. Atmos. Sol. Terr. Phys. 59 (11), 1225–1232.
Taricco, C., Arnone, E., Rubinetti, S., Bizzarri, I., Agafonova, N.Y., Aglietta, M., Antonioli, P., Ashikhmin, V.V., Bari, G., Bruno, G., Dobrynina, E.A., Enikeev, R.I., Fulgione, W., Galeotti, P., Garbini, M., Ghia, P.L., Giusti, P., Kemp, E., Malgin, A.S., Molinario, A., Persiani, R., Pless, I.A., Ryazhskaya, O.G., Sartorelli, G., Shakiryanova, I.R., Selvi, M., Trinchero, G.C., Vigorito, C.F., Yakushev, V.F., A. z.,, 2022. Exploration of the stratosphere with cosmic-ray muons detected underground. Phys. Rev. Res. 4 (2).
Thompson, D.W.J., Wallace, J.M., Jones, P.D., Kennedy, J.J., 2009. Identifying signatures of natural climate variability in time series of global-mean surface temperature: Methodology and insights. J. Clim. 22 (22), 6120–6141.
Todd, M.C., Kniveton, D.R., 2001. Changes in cloud cover associated with forbush decreases of galactic cosmic rays. J. Geophys. Res. Atmos. 106 (D23), 32031–32041.
Vahrenholt, F., Lüning, S., 2013. The neglected sun - why the sun precludes climate catastrophe. Stacey International.
Vieira, L.E.A., Solanki, S.K., Krivova, N.A., Usoskin, I., 2011. Evolution of the solar irradiance during the holocene. Astron. Astrophys. 531, A6.
Wang, Y.-M., Lean, J.L., Sheeley, N.R., 2005. Modeling the sun's magnetic field and irradiance since 1713. Astrophys. J. 625 (1), 522–538.
Willson, R.C., 1997. Total solar irradiance trend during solar cycles 21 and 22. Science 277 (5334), 1963–1965.
Willson, R.C., Mordvinov, A.V., 2003. Secular total solar irradiance trend during solar cycles 21–23. Geophys. Res. Lett. 30 (5), 1199.
Wu, C.-J., Krivova, N.A., Solanki, S.K., Usoskin, I.G., 2018. Solar total and spectral irradiance reconstruction over the last 9000 years. Astron. Astrophys. 620, A120.
Wyatt, M.G., Curry, J.A., 2013. Role for Eurasian arctic shelf sea ice in a secularly varying hemispheric climate signal during the 20th century. Clim. Dyn. 42 (9–10), 2763–2782.
Yeo, K.L., Ball, W.T., Krivova, N.A., Solanki, S.K., Unruh, Y.C., Morrill, J., 2015. UV solar irradiance in observations and the NRLSSI and SATIRE-s models. J. Geophys. Res. Space Phys. 120 (8), 6055–6070.
Yeo, K.L., Solanki, S.K., Krivova, N.A., Rempel, M., Anusha, L.S., Shapiro, A.I., Tagirov, R.V., Witzke, V., 2020. The dimmest state of the sun. Geophys. Res. Lett. 47 (19). e2020GL090243.
Zacharias, P., 2014. An independent review of existing total solar irradiance records. Surv. Geophys. 35 (4), 897–912.
Ziskin, S., Shaviv, N.J., 2012. Quantifying the role of solar radiative forcing over the 20th century. Adv. Space Res. 50 (6), 762–776.